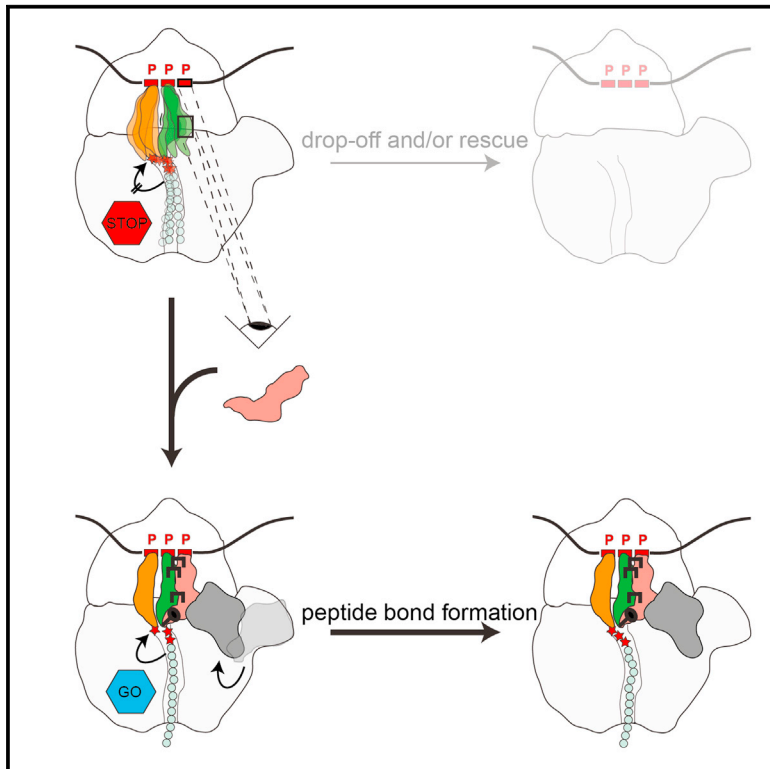Article

Structural Basis for Polyproline-Mediated Ribosome Stalling and Rescue by the Translation Elongation Factor EF-P

Graphical Abstract

Authors

Paul Huter, Stefan Arenz,
Lars V. Bock, ..., Marina V. Rodnina,
Andrea C. Vaiana, Daniel N. Wilson

Correspondence

daniel.wilson@chemie.uni-hamburg.de

In Brief

Huter et al. present cryo-EM structures of polyproline-stalled ribosomes in the presence and absence of translation elongation factor EF-P. The structures reveal that polyproline sequences arrest translation by destabilizing the P-site tRNA, whereas binding of EF-P stabilizes the P-site tRNA and promotes a favorable geometry for peptide bond formation.

Highlights

- Polyproline-containing peptides stall translation by destabilizing the P-site tRNA

- Elongation factor EF-P recognizes the P-site tRNA and E-site mRNA codon

- The lysine modification of EF-P stabilizes the CCA end of the P-site tRNA

- EF-P promotes a favorable geometry of the P-site for peptide bond formation

CrossMark

CellPress

Article

Structural Basis for Polyproline-Mediated Ribosome Stalling and Rescue by the Translation Elongation Factor EF-P

Paul Huter,[1] Stefan Arenz,[1] Lars V. Bock,[2] Michael Graf,[1] Jan Ole Frister,[3] Andre Heuer,[1] Lauri Peil,[4] Agata L. Starosta,[1,7] Ingo Wohlgemuth,[3] Frank Peske,[3] Jiří Nováček,[5] Otto Berninghausen,[1] Helmut Grubmüller,[2] Tanel Tenson,[4] Roland Beckmann,[1] Marina V. Rodnina,[3] Andrea C. Vaiana,[2] and Daniel N. Wilson[1,6,8,*]

[1]Gene Center, Department for Biochemistry and Center for integrated Protein Science Munich (CiPSM), University of Munich, Feodor-Lynenstr. 25, 81377 Munich, Germany
[2]Department of Theoretical and Computational Biophysics, Max Planck Institute for Biophysical Chemistry, Am Fassberg 11, Göttingen 37077, Germany
[3]Department of Physical Biochemistry, Max Planck Institute for Biophysical Chemistry, Am Fassberg 11, 37077 Göttingen, Germany
[4]University of Tartu, Institute of Technology, Nooruse 1, 50411 Tartu, Estonia
[5]Central European Institute of Technology (CEITEC), Masaryk University, Kamenice 5, 62500 Brno, Czech Republic
[6]Institute for Biochemistry and Molecular Biology, University of Hamburg, Martin-Luther-King-Platz 6, 20146 Hamburg, Germany
[7]Present address: Centre for Bacterial Cell Biology, Institute for Cell and Molecular Biosciences, University of Newcastle, Newcastle upon Tyne NE2 4AX, UK
[8]Lead Contact
*Correspondence: daniel.wilson@chemie.uni-hamburg.de
https://doi.org/10.1016/j.molcel.2017.10.014

SUMMARY

Ribosomes synthesizing proteins containing consecutive proline residues become stalled and require rescue via the action of uniquely modified translation elongation factors, EF-P in bacteria, or archaeal/eukaryotic a/eIF5A. To date, no structures exist of EF-P or eIF5A in complex with translating ribosomes stalled at polyproline stretches, and thus structural insight into how EF-P/eIF5A rescue these arrested ribosomes has been lacking. Here we present cryo-EM structures of ribosomes stalled on proline stretches, without and with modified EF-P. The structures suggest that the favored conformation of the polyproline-containing nascent chain is incompatible with the peptide exit tunnel of the ribosome and leads to destabilization of the peptidyl-tRNA. Binding of EF-P stabilizes the P-site tRNA, particularly via interactions between its modification and the CCA end, thereby enforcing an alternative conformation of the polyproline-containing nascent chain, which allows a favorable substrate geometry for peptide bond formation.

INTRODUCTION

Ribosomes catalyze the synthesis of proteins in cells by providing a platform for the binding of tRNAs. There are three tRNA binding sites on the ribosome, the A, P, and E sites. During translation elongation, aminoacyl-tRNAs (aa-tRNAs) binding at the A site undergo peptide bond formation with the peptidyl-

tRNA located at the P site. The rate of peptide bond formation is influenced by the chemical nature of the amino acid substrates in both the A and P sites. Among other amino acids, proline is a particularly poor substrate both as donor and acceptor during peptide bond formation (Pavlov et al., 2009; Johansson et al., 2011; Muto and Ito, 2008; Wohlgemuth et al., 2008; Doerfel et al., 2013, 2015). In fact, ribosomes become stalled when synthesizing proteins containing consecutive proline residues (Doerfel et al., 2013; Ude et al., 2013; Woolstenhulme et al., 2013). To alleviate the ribosome stalling and allow translation to continue, a specialized translation factor is required, elongation factor P (EF-P) in bacteria or initiation factor 5A (IF5A) in archaea and eukaryotes (Doerfel et al., 2013; Ude et al., 2013; Gutierrez et al., 2013). IF5A has been shown to be essential in eukaryotes (Dever et al., 2014), and deletion of *efp* in some bacteria leads to growth defects and avirulence (Lassak et al., 2016).

Both EF-P and IF5A bear post-translational modifications that are essential for their rescue activity (Doerfel et al., 2013; Ude et al., 2013; Gutierrez et al., 2013; Peil et al., 2013). In *Escherichia coli*, lysine 34 (K34) of EF-P is post-translationally modified by the combined action of EpmA (YjeA), EpmB (YjeK), and EpmC (YfcM). EpmB converts (S)-α-lysine to (R)-β-lysine (Behshad et al., 2006), and EpmA ligates the (R)-β-lysine to the ε-amino group of K34 (Yanagisawa et al., 2010; Navarre et al., 2010). EpmC recognizes the modified form of EF-P and hydroxylates the C5(δ) of K34 (Peil et al., 2012); however, the hydroxylation is not required for the rescue activity of EF-P (Doerfel et al., 2013; Ude et al., 2013). Surprisingly, the resulting ε(R)-β-lysyl-hydroxylysine modification of *E. coli* EF-P and the enzymes associated with this modification are not conserved across all bacteria (Bailly and de Crécy-Lagard, 2010; Lassak et al., 2015). Instead, unrelated enzymes and/or modifications have been identified in other bacteria. In *Pseudomonas aeruginosa* and *Shewanella oneidensis*, EarP catalyzes the addition of
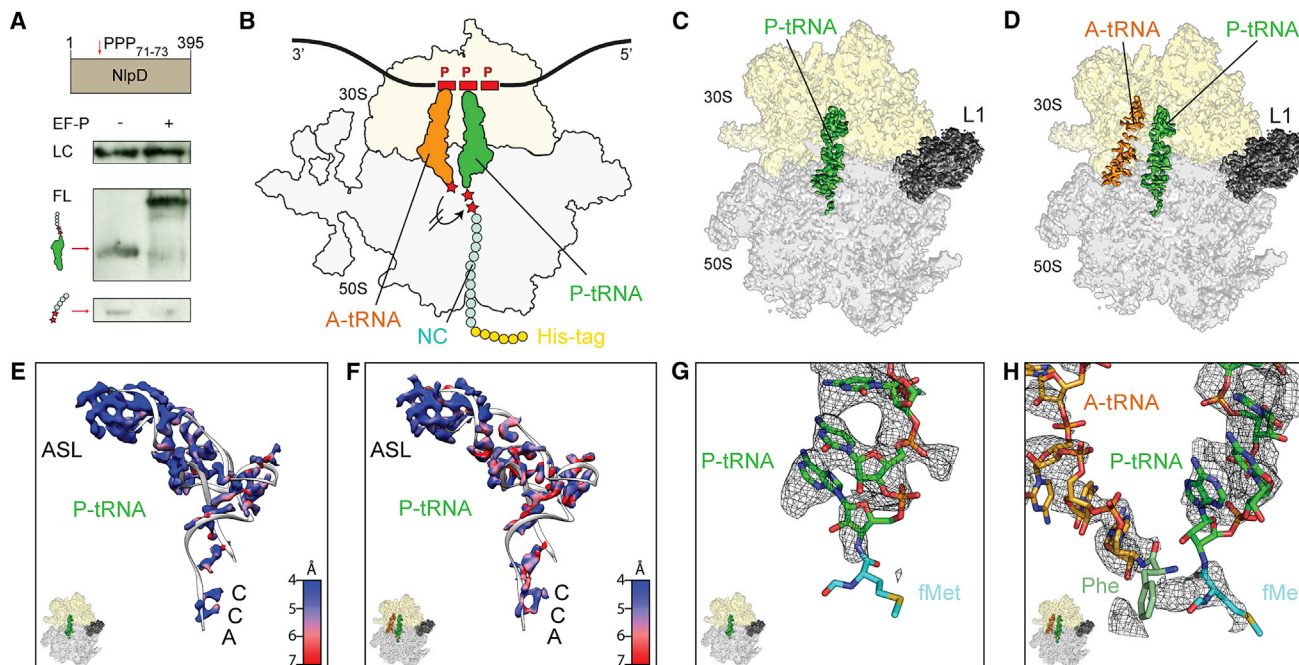
Figure 1. Cryo-EM Structures of Polyproline-Stalled Ribosomes in the Absence of EF-P

(A) Schematic representation of NlpD-PPP reporter protein (brown) with the site of the PPP-motif indicated. Western blot using an anti-HA-tag antibody of *in vitro* translation reactions of NlpD-PPP reporter in the absence (–) and presence (+) of EF-P. Full-length (FL), peptidyl-tRNA, and free peptide, as well as loading control (LC), are indicated.

(B–D) Schematic representation (B) and cryo-EM reconstructions (C and D) of PPP-stalled ribosome complexes formed in the absence of EF-P containing P-tRNA (C) or A- and P-tRNAs (D). The nascent chain (NC) has an N-terminal histidine tag (His-tag).

(E and F) Cryo-EM density at high threshold (7σ), colored according to the local resolution, for the P-site tRNA (gray ribbon) from cryo-EM maps in (C) containing P-tRNA (E) and in (D) containing A- and P-tRNAs (F), respectively.

(G) Cryo-EM density (mesh) of the CCA end of the P-site tRNA (green) from (C), with aligned fMet (cyan, PDB: 1VY4) (Polikanov et al., 2014) illustrating lack of density for nascent chain even at low thresholds (4σ).

(H) Cryo-EM density (mesh) of the CCA end of the A-site tRNA (orange) and P-site tRNA (green) from (D), with aligned Phe (green) and fMet (cyan, PDB: 1VY4) (Polikanov et al., 2014).

See also Figures S1 and S2.

rhamnose to arginine 32 (R32) of EF-P (Lassak et al., 2015; Rajkovic et al., 2015), whereas *Bacillus subtilis* is reported to bear a 5-aminopentanol moiety attached to K32 (Rajkovic et al., 2016). In eukaryotes, a conserved lysine residue is post-translationally modified to hypusine by the action of deoxyhypusine synthase (DHS) and deoxyhypusine hydroxylase (DOHH) (Dever et al., 2014; Lassak et al., 2016).

The structure of bacterial EF-P revealed a three-domain architecture, with the modified residue located at the tip of domain 1 (Hanawa-Suetsugu et al., 2004). aIF5A and eIF5A are homologous to bacterial EF-P domains 1 and 2 but lack the bacterial-specific domain 3 (Dever et al., 2014; Lassak et al., 2016). The X-ray structure of unmodified *Thermus thermophilus* EF-P in complex with *T. thermophilus* 70S ribosome bearing a deacylated tRNA^fMet at the P site revealed that EF-P binds within the E site of the ribosome with the unmodified arginine 32 (R32) of EF-P interacting with the CCA end of the P-site tRNA (Blaha et al., 2009). Similarly, structures of modified eIF5A on the yeast ribosome also visualized the hypusine modification extending into the peptidyltransferase center (PTC) of the ribosome (Melnikov et al., 2016b; Schmidt et al., 2016), where it interacts with the

CCA end of the P-site tRNA (Schmidt et al., 2016). However, to date, no structures exist of EF-P or eIF5A in complex with polyproline-stalled ribosomes; therefore, it remains unclear how the proline residues stall translation and how EF-P/IF5A alleviates these stalled ribosomes.

RESULTS

Structure of a Polyproline-Stalled Ribosome Complex

To investigate how polyproline stretches cause translational arrest, we employed a previously used reporter mRNA coding for NlpD-PPP protein bearing three consecutive proline (71PPP73) residues (Starosta et al., 2014) (Figure 1A), which was translated in an *E. coli* lysate-based translation system derived from an *E. coli efp* deletion strain (see STAR Methods). As expected (Starosta et al., 2014), ribosomes with peptidyl-tRNA stalled at the PPP stretch could be alleviated by the exogenous addition of purified modified EF-P protein (Figure 1A). Previous biochemical studies (Doerfel et al., 2013; Ude et al., 2013; Woolstenhulme et al., 2013), as well as toeprinting assays using the same NlpD-PPP template (Starosta et al., 2014), indicate that

Table 1. Cryo-EM Data Collection, Refinement, and Validation Statistics

	#1 P-site tRNA only (EMDB: 3898, PDB: 6ENF)	#2 A- and P-site tRNA + EF-P (EMDB: 3899, PDB: 6ENJ)	#3 P-site tRNA + EF-P (EMDB: 3903, PDB: 6ENU)
Data Collection			
Microscope	FEI Titan Krios	FEI Titan Krios	FEI Titan Krios
Camera	Falcon II	Falcon II	Falcon II
Magnification	129,151	129,151	129,151
Voltage (kV)	300	300	300
Electron dose ($e^-/Å^2$)	28	28	28
Defocus range (μm)	−0.8 to −2.5	−0.8 to −2.5	−0.8 to −2.5
Pixel size (Å)	1.084	1.084	1.084
Initial particles (no.)	229,613	229,613	229,455
Final particles (no.)	75,089	21,655	69,761
Model Composition			
Protein residues	5,531	5,951	5,944
RNA bases	4,547	4,693	4,613
Refinement			
Resolution range (Å)	3.3	3.9	3.2
Map CC (around atoms)	0.78	0.72	0.80
Map CC (whole unit cell)	0.76	0.75	0.75
$FSC_{average}$	0.85	0.85	0.85
Map sharpening B factor ($Å^2$)	−62,88	−66,61	−60,10
RMS Deviations			
Bond lengths (Å)	0.011	0.003	0.007
Bond angles (°)	0.729	0.594	0.932
Validation			
MolProbity score	1.77	1.64	1.77
Clashscore	4.29	3.44	4.11
Poor rotamers (%)	0	0.04	0.41
Ramachandran Plot			
Favored (%)	92.06	91.33	88.83
Allowed (%)	7.76	8.37	10.74
Disallowed (%)	0.18	0.31	0.43

ribosomes stall in the absence of EF-P because of slow peptide bond formation between the peptidyl-Pro-Pro-tRNA in the P site and the incoming Pro-tRNA in the A site (Figure 1B). These PPP-stalled ribosomes were purified using the 6x-Histidine tag located at the N terminus of the nascent peptide (Figure 1B) and subjected to cryo-electron microscopy (cryo-EM) analysis (see STAR Methods). *In silico* sorting of the cryo-EM images yielded two subpopulations of non-rotated ribosomes bearing a P-site tRNA but differing by the absence or presence of A-site tRNA (44% and 17%, respectively; Figure S1A). The cryo-EM structures were refined to yield average resolutions of 3.6 Å and 3.9 Å, respectively (Figures 1C and 1D; Figures S1B–S1E; Table 1). In addition, a large population (30%) of vacant ribosomes was observed, as well as a small population (9%) of 70S ribosomes in a rotated state lacking EF-P but containing hybrid A/P-site and P/E-site tRNAs (Figure S1A), the latter presumably representing a post-peptide bond formation state.

The density quality and resolution for the A-site and P-site tRNAs were generally poorer and less uniform than observed in previous ribosomal complexes (Arenz et al., 2014a, 2014b, 2016a). In particular, the density was well resolved for the anti-codon stem loop (ASL) of the tRNA on the 30S subunit and progressively deteriorated toward the elbow and acceptor arm of the tRNAs on the 50S subunit (Figures 1E and 1F; Figures S2A–S2G). In fact, density for the CCA end of the P- and A-site tRNAs at the PTC was only present at low thresholds (Figures 1G and 1H). Local resolution calculations also confirmed the flexible nature of the CCA end, particularly with respect to the terminal A76 nucleotide (Figures S2H–S2J). In the structure containing only P-site tRNA, no significant density was observed for the nascent polypeptide chain (Figure 1G), whereas in the structure with both A- and P-site tRNAs, the density attributable to the nascent chain was fragmented and disconnected from the tRNAs (Figure 1H). The density for the CCA end of the A-site tRNA was worse than the one of the P-site tRNA (Figure 1D; Figures S2D–S2G), suggesting that the Pro-tRNA had severe problems to accommodate at the A site of the PTC. Consistent with this notion, the N terminus of ribosomal protein L27, which
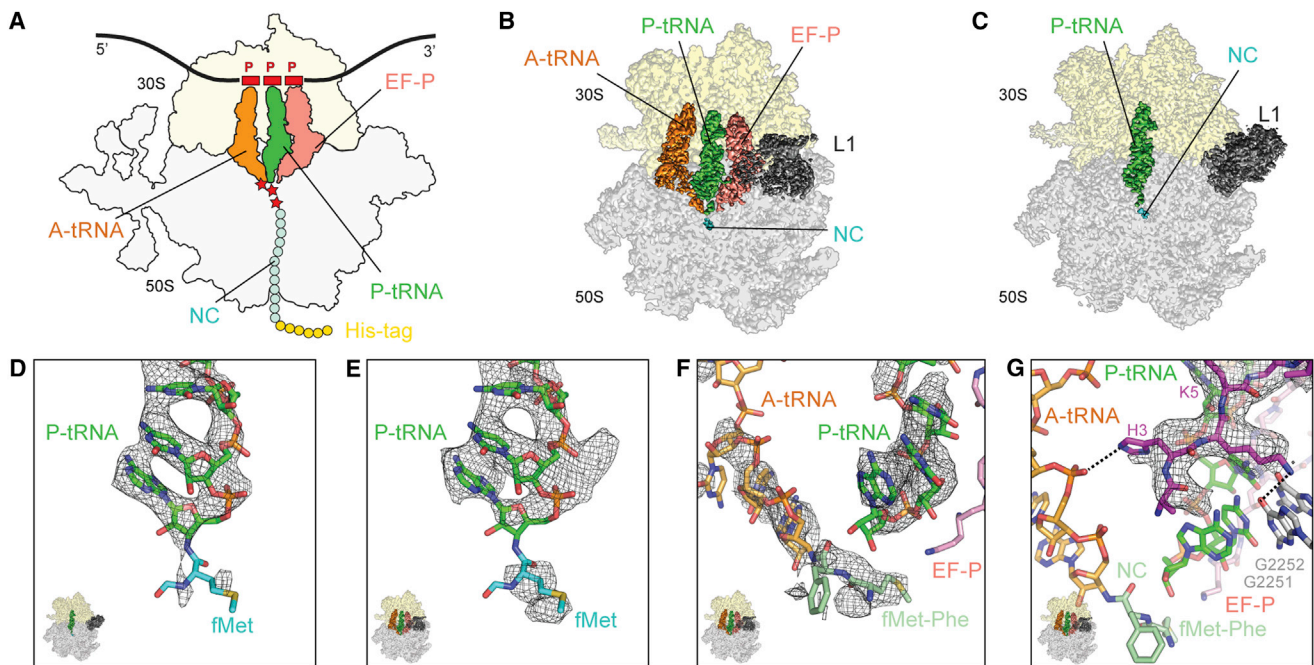
Figure 2. Cryo-EM Structures of Polyproline-Stalled Ribosomes in the Presence of EF-P

(A–C) Schematic representation (A) and cryo-EM reconstructions (B and C) of PPP-stalled ribosome complexes with (B) or without (C) of EF-P (salmon) bound in the E site.

(D and E) Cryo-EM density (mesh) of the CCA end of the P-site tRNA (green) from cryo-EM maps in (C) without EF-P (D) and in (B) with EF-P (E), respectively, with aligned fMet (cyan, PDB: 1VY4) (Polikanov et al., 2014).

(F) Cryo-EM density (mesh) of the CCA end of the A-site tRNA (orange) and P-site tRNA (green) from (B), with aligned fMet-Phe dipeptide (green, PDB: 1VY5) (Polikanov et al., 2014).

(G) Cryo-EM density (mesh) for the N-terminal residues of L27 (purple) showing possible interactions with residues G2251 and G2252 of the P loop (gray) and A-site tRNA (orange).

See also Figure S1.

becomes stabilized upon A-site tRNA accommodation (Polikanov et al., 2014; Voorhees et al., 2009), remained disordered (Figure S2K). Collectively, our findings suggest that the presence of the polyproline stretch within the nascent polypeptide chain leads to destabilization of the peptidyl-tRNA and prevents accommodation of the aa-tRNA at the A site, thereby causing translational stalling.

EF-P in Complex with PPP-Stalled Ribosomes

To investigate structurally how EF-P relieves the translation arrest caused by polyproline stretches, we incubated PPP-stalled ribosomes with fully modified *E. coli* EF-P (Figure 2A) and analyzed the resulting complexes by cryo-EM. *In silico* sorting of the cryo-EM data yielded two major subpopulations of ribosomes bearing P-site tRNA, distinguished by the presence (30%) or absence (33%) of EF-P (Figure S1F). The EF-P-containing subpopulation was extremely heterogeneous, and only a stable subpopulation containing A- and P-site tRNAs with EF-P bound in the E site (Figure 2B) could be refined further, yielding an average resolution of 3.7 Å (Figures S1G and S1H; Table 1). Despite multiple attempts, we were unable to obtain a clean subpopulation containing P-site tRNA and EF-P but lacking A-site tRNA. For completeness, we also refined the major P-site tRNA subpopulation lacking EF-P (Figure 2C) to an average

resolution of 3.2 Å (Figures S1I and S1J; Table 1). As before (Figure 1G), little density was observed for the nascent polypeptide chain attached to the P-site tRNA in the EF-P-lacking structure (Figure 2D) despite the improved quality of the density for the CCA end of the P-site tRNA. By contrast, additional nascent chain density was observed when EF-P was present (Figure 2E); however, this density fused directly to the A-site tRNA rather than the P-site tRNA (Figure 2F). Therefore, we concluded that the EF-P-containing subpopulation represents a post-peptide bond formation state with deacylated tRNA in the P site and peptidyl-tRNA in the A site. We also observe that the N terminus of L27 was ordered (Figure 2G), which, as mentioned, is diagnostic for accommodation of the aa-tRNA at the A site (Polikanov et al., 2014; Voorhees et al., 2009).

EF-P in Complex with PP-Stalled Ribosomes without the A-Site tRNA

In order to capture EF-P bound to polyproline-stalled ribosomes in a pre-peptide bond formation state, we employed a modified version of the NlpD-PPP mRNA that was truncated directly after the codon for the second proline of the PPP motif (Figure 3A). Ribosomes translating the truncated NlpD-PP mRNA become stalled after the PP motif because the absence of an A-site codon precludes binding of the next aa-tRNA; thus, the
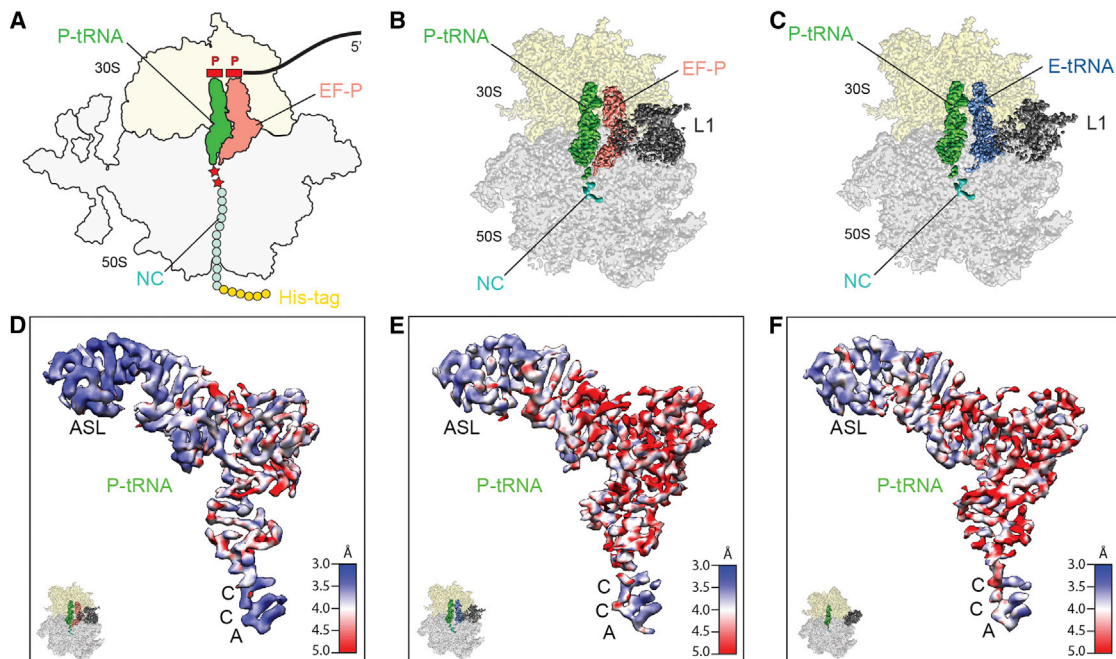
Figure 3. Stabilization of the P-Site Peptidyl-tRNA by EF-P

(A–C) Schematic representation (A) and cryo-EM reconstructions (B and C) of truncated NlpD-PP-stalled ribosomes in the presence (B) or absence (C) of EF-P (salmon).

(D–F) Cryo-EM densities colored according to local resolution for the P-site tRNAs from reconstructions illustrated in (B) and (C), respectively, (D and E) as well as from the reconstruction from Figure 2C (F).

See also Figure S1.

ribosomes cannot catalyze peptide bond formation even when EF-P is present (Figure 3A). The purified truncated NlpD-PP-stalled ribosomes were then incubated with active modified *E. coli* EF-P (Figure 3A), and the resulting complexes were analyzed by cryo-EM. *In silico* sorting of the cryo-EM data yielded two major subpopulations of ribosomes bearing either P- and E-site tRNAs (22%) or P-site tRNA with EF-P bound in the E site (74%) (Figure S1K). The EF-P-containing subpopulation could be further segregated into ribosome populations that differed with respect to the L1 stalk adopting an "in" (30%) or "out" (44%) conformation. The "in" position of the L1 stalk significantly improved the quality of the EF-P density, and therefore this population was further refined, yielding a final cryo-EM structure (Figure 3B) with an average resolution of 3.1 Å (Figures S1L and S1M; Table 1). Similarly, we could also refine the major P- and E-site tRNA-containing ribosome subpopulation that lacked EF-P (Figure 3C) to a final average resolution of 3.2 Å (Figures S1N and S1O). Local resolution calculations indicate less flexibility of the P-site tRNA in the presence of EF-P (Figure 3D) when compared to ribosomes bound with E-site tRNA (Figure 3E) or having a vacant E site (Figure 3F), thus supporting the hypothesis that EF-P stabilizes the P-site peptidyl-tRNA on the ribosome.

EF-P Residues Critical for P-Site tRNA Interaction

The well-resolved density for *E. coli* EF-P bound to the ribosome population with the L1 "in" conformation enabled a complete molecular model to be generated (Figure 4A; Figure S3A). The overall conformation of *E. coli* EF-P on a polyproline-stalled ribosome is very similar to that observed by X-ray crystallography for *T. thermophilus* EF-P bound to a *T. thermophilus* 70S ribosome with a deacylated-tRNA^{fMet} in the P site (Blaha et al., 2009), whereas it deviates more significantly from the binding position observed for the yeast homolog eIF5A bound to the 80S ribosome (Schmidt et al., 2016; Melnikov et al., 2016b) (Figures S3B and S3C). We observe that the backbone of Asp69 of *E. coli* EF-P is within hydrogen bonding distance of U17a within the D-loop of the peptidyl-tRNA^{Pro} in the P site (Figure S3D). This interaction is also observed in the *T. thermophilus* EF-P-ribosome structure (Blaha et al., 2009) (Figure S3E) but is not possible for tRNAs containing shorter D-loops (Figure S3F), thus providing a specificity determinant for EF-P to recognize tRNA^{fMet} and tRNA^{Pro} (Katoh et al., 2016) (Figures S3D and S3E). By contrast, such a specific interaction between yeast eIF5A and the P-site tRNA was not observed (Schmidt et al., 2016; Melnikov et al., 2016b), consistent with the diverse range of non-proline-containing stalling motifs that are recognized and rescued by eIF5A (Schuller et al., 2017; Pelechano and Alepuz, 2017).

Unlike eIF5A, bacterial EF-P has an additional domain 3 that contacts the small ribosomal subunit and the ASL of the P-site tRNA (Figure 4B). In particular, two conserved residues Tyr183 and Arg186 are within hydrogen bonding distance of A42 of the P-site tRNA and G1338 within helix h29 of the 16S rRNA
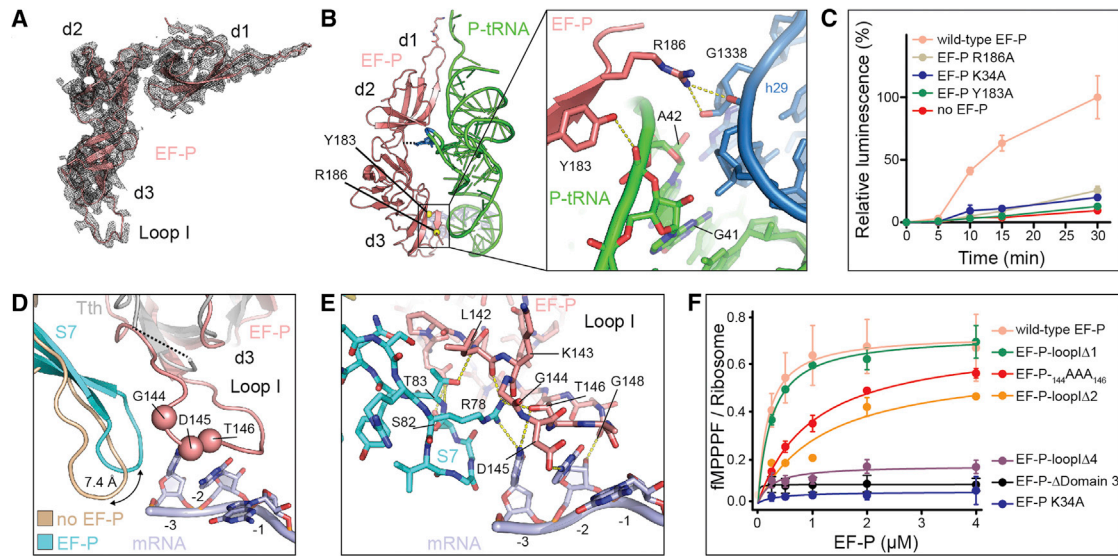
Figure 4. Interaction of EF-P with the P-Site tRNA

(A) Cryo-EM density (mesh) with molecular model for EF-P (salmon ribbon) with domains 1–3 (d1–d3) indicated.

(B) Overview of EF-P relative to P-site-bound tRNA^{Pro} (green) with a zoom on the interactions between Y183 and R186 of EF-P and their respective interaction partners of tRNA^{Pro} and h29 (blue) of the 30S subunit.

(C) Luminescence resulting from *in vitro* translated Fluc-3xPro was monitored over time and quantified in the absence of EF-P (red) or in the presence of wild-type EF-P (pink) or indicated EF-P variants. 100% luminescence is defined as the luminescence produced by Fluc-3xPro after a 30-min incubation in the presence of wild-type EF-P. Error bars represent the standard deviation of three independent experiments.

(D) Location of EF-P d3 loop I relative to peptidyl-tRNA^{Pro} (green) in the P site, mRNA (light blue), and ribosomal protein S7 (cyan), with the position of the loop of S7 in the absence of EF-P (tan) indicated for reference. The relative position of *T. thermophilus* EF-P (Blaha et al., 2009) (gray) is shown with the disordered region of d3 loop of EF-P indicated (dashed line). The positions of the conserved residues within the $_{144}$GDT$_{146}$ motif within loop I of EF-P are indicated by spheres.

(E) Potential hydrogen-bond interactions (dashed yellow lines) between Loop I of EF-P (salmon), the E-site codon (blue), and S7 (cyan).

(F) Synthesis of the fMPPPF peptide as a function of EF-P concentration in the presence of wild-type EF-P (pink) or various EF-P variants. In the absence of EF-P, 0.06 ± 0.01 fMPPPF peptide were formed per ribosome. Error bars represent the standard deviation of three independent experiments.

See also Figures S3–S5.

(Blaha et al., 2009) (Figure 4B). To investigate the importance of these interactions, we generated modified EF-P variants bearing Y183A or R186A substitutions and monitored their ability to promote translation of a polyproline-containing firefly luciferase (Fluc) reporter protein (Ude et al., 2013) (Figure 4C). In the absence of EF-P, ribosomes stall at the polyproline motif and little or no luminescence is observed because translation of full-length Fluc is prevented. As expected, addition of modified wild-type EF-P rescues the polyproline-stalled ribosomes, leading to production of full-length Fluc and a corresponding increase in luminescence (Figure 4C). By contrast, the EF-P-Y183A and EF-P-R186A variants were both completely inactive, as was the previously reported inactive EF-P-K34A variant (Ude et al., 2013). These findings demonstrate that the Tyr183 and Arg186 residues are critical for the rescue activity of EF-P and explain their high conservation among bacterial EF-P proteins.

Interaction of EF-P with the mRNA Codon in the E Site

In the X-ray structure of *T. thermophilus* EF-P-ribosome structure, loop I of domain 3 of EF-P is disordered (Blaha et al., 2009) (Figure 4D). By contrast, loop I is well resolved in the cryo-EM structure of *E. coli* EF-P in complex with the PP-stalled ribosome (Figure 4A; Figures S4A and S4B), where it interacts with the ribosomal protein S7 and E-site codon of the mRNA

(Figures 4D and 4E). Binding of EF-P to the ribosome leads to a shift in conformation of the β-hairpin of S7 by 7.4 Å (Figure 4D), which is stabilized via potential hydrogen bond interactions between the sidechain of Arg78 of S7 and the backbone of Gly144 as well as the sidechain of T146 of EF-P (Figure 4E). Additional interactions are formed between S7 (Thr83 and Ser82) and EF-P (the backbone of Leu142 and the side chain of Asp139) (Figure 4E; Figures S4C and S4D). Loop I of domain 3 of EF-P contains a highly conserved Gly144-Asp145-Thr146 (GDT) motif, which establishes contact with the nucleobase of the first and second positions of the E-site codon of the mRNA (Figures 4D and 4E; Figures S4E and S4F). To assess the importance of the GDT motif for EF-P activity, we generated modified EF-P bearing a triple substitution of GDT to AAA (EF-P-$_{144}$AAA$_{146}$). Since most of the interactions involve the backbone of the GDT motif, we also generated EF-P variants where 1, 2, or 4 residues within loop I were deleted (EF-P-loopIΔ1, -loopIΔ2, and -loopIΔ4, respectively). The activity of the EF-P variants was assessed by monitoring the formation of fMPPPF peptide on the ribosome, as described previously (Doerfel et al., 2013, 2015). As seen in Figure 4F, no fMPPPF peptide was synthesized when the inactive EF-P-K34A variant was used (or when EF-P was absent, see legend to Figure 4), whereas the presence of wild-type EF-P led to efficient fMPPPF peptide formation.
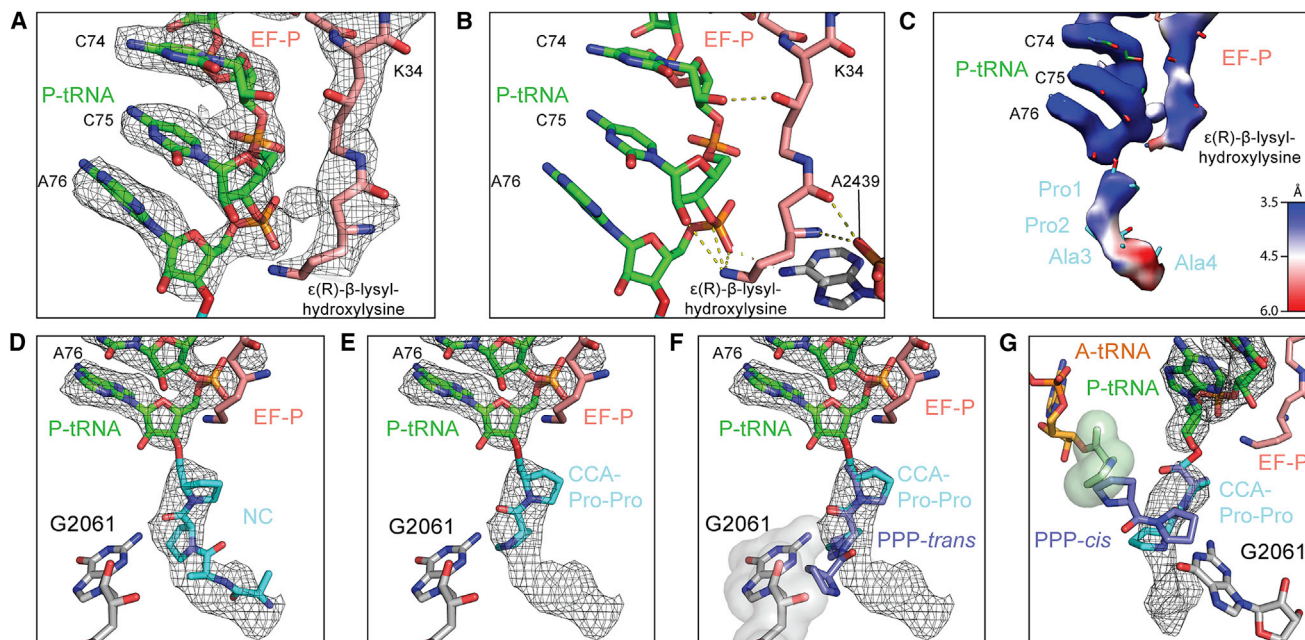
Figure 5. EF-P Stabilizes the PP-Containing Nascent Chain

(A) Cryo-EM density (gray mesh) for the CCA end of the P-site tRNA (green) and ε(R)-β-lysyl-hydroxylysine modification of EF-P (salmon).

(B) Same as (A), but without cryo-EM density, and potential hydrogen bond interactions (dashed lines) between the ε(R)-β-lysyl-hydroxylysine modification, P-site tRNA (green), and A2439 (gray) are indicated.

(C) Cryo-EM density colored according to the local resolution for the CCA end of the P-site tRNA, ε(R)-β-lysyl-hydroxylysine modification of EF-P, and the modeled nascent chain (Pro1-Pro2-Ala3-Ala4).

(D–G) Cryo-EM density (mesh) for the P-site tRNA with the first four residues of the modeled nascent chain (NC) Pro1-Pro2-Ala3-Ala4 (cyan) (D), all-*trans* Pro-Pro conformation of CCA-Pro-Pro tRNA mimic in complex with yeast 80S ribosome (PDB: 5DGV) (Melnikov et al., 2016a) (E), three prolines of a polyproline type II (P$_{II}$) helix (PP-*trans*) modeled onto the CCA end of the P-site tRNA, with G2061 shown as a surface to better illustrate the steric clash with the PP-*trans* nascent chain (F), and three prolines of a polyproline type I (P$_I$) helix (PP-*cis*) modeled onto CCA end of the P-site tRNA (G), showing a potential clash with a Pro residue (light green surface) attached to the A-site tRNA (orange).

See also Figure S6.

While the EF-P-loopIΔ1 retained wild-type-like activity, the EF-P-$_{144}$AAA$_{146}$ and EF-P-loopIΔ2 variants displayed reduced activity, and the EF-P-loopIΔ4 variant was completely inactive (Figure 4F). Furthermore, an EF-P variant with the complete domain 3 deleted (EF-P-ΔDomain 3) was also inactive (Figure 4F).

These results suggest that the conserved loop I of domain 3 of EF-P is critical for the rescue activity of EF-P and raises the possibility that EF-P recognizes the nature of the E-site codon, analogous to stop codon recognition by the SPF and PXT containing loops of termination factors RF2 and RF1, respectively (Zhou et al., 2012). Modeling on the basis of our structure suggests that purines in the first and second position, such as AAA or GGG codons, in the E site lead to clashes with EF-P, whereas UUU could be accommodated but in a less stable manner (Figures S5A–S5D). In the X-ray structure of *T. thermophilus* EF-P-ribosome structure, the E-site codon was AAA (Blaha et al., 2009) (Figures S5E and S5F), possibly explaining why loop I of domain 3 of EF-P was disordered. Moreover, the −3 nucleotide was also not visualized, supporting the suggestion that EF-P is critical for positioning and stabilization of the E-site codon (Figures S5E and S5F). Further biochemical experiments will be necessary to assess whether loop I of EF-P can really distinguish

CCN proline codons in the E site from other sense codons. The absence of domain 3 in eIF5A does, however, preclude recognition of the nature of the E-site codon, which may contribute to the relaxed specificity of eIF5A, allowing eIF5A to also act on a diverse range of non-proline containing stalling motifs (Schuller et al., 2017; Pelechano and Alepuz, 2017).

Stabilization of the CCA End of the P-Site tRNA by the EF-P Modification

Clear electron density is observed at the tip of domain 1 of EF-P that corresponds to the ε(R)-β-lysylhydroxylysine located at position K34 of EF-P (Figures 5A and 5B). The post-translational modification extends into a crevice located adjacent to the CCA end of the P-site tRNA (Figures 5A and 5B), similar but distinct from that observed previously for the unmodified R32 residues of *T. thermophilus* EF-P (Blaha et al., 2009), and the hypusine modification located at position K51 of yeast eIF5A (Schmidt et al., 2016; Melnikov et al., 2016b) (Figures S3G–S3I). The structure reveals how the EF-P modification can stabilize the P-site tRNA (Figure 5C) by forming interactions with the backbone of the CCA end (Figure 5B). Specifically, hydrogen bonds are possible between the ε-amino group of the (R)-lysyl moiety of EF-P and the 2′ OH of the ribose of C75 and the bridging oxygen
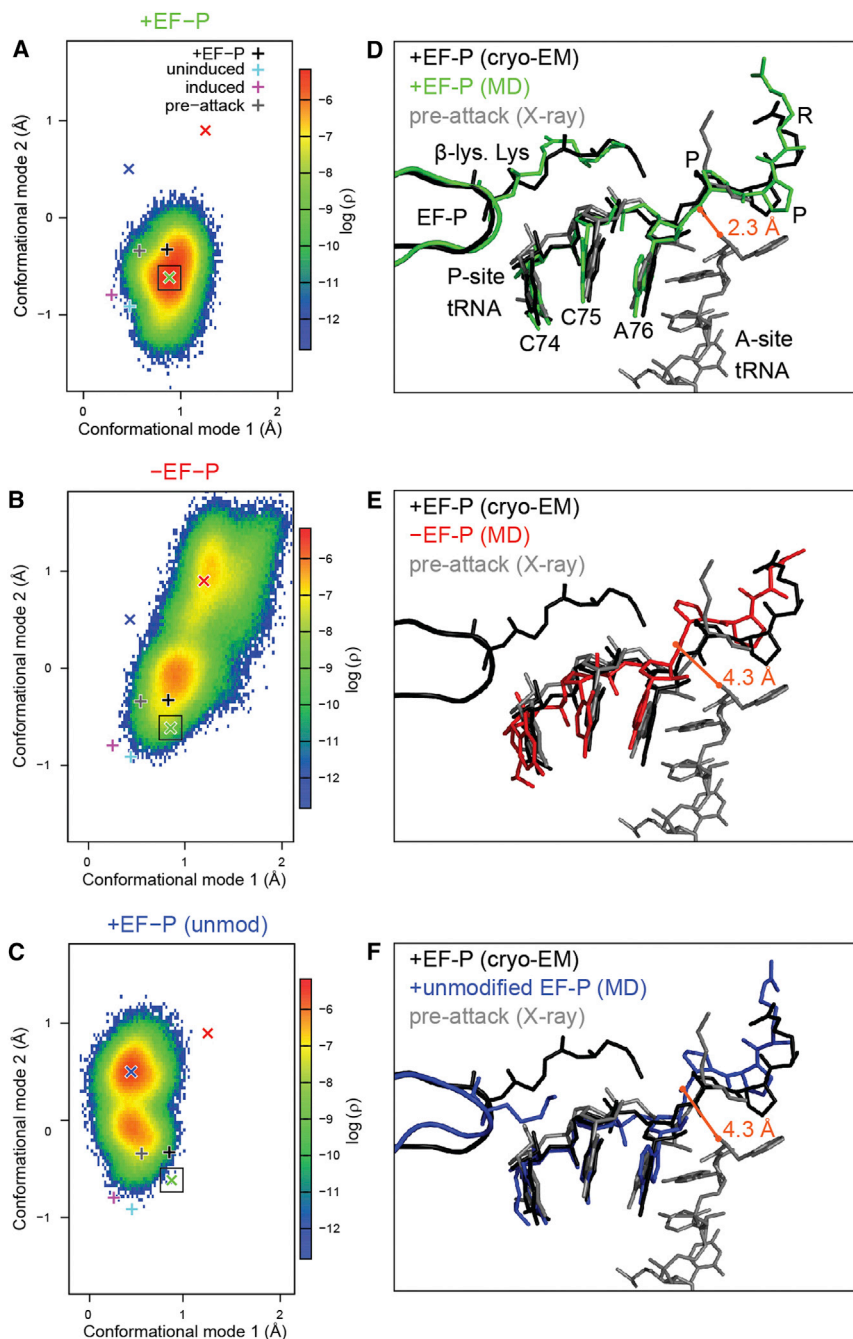
Figure 6. MD Simulations of Polyproline-Stalled Ribosomes in the Presence and Absence of EF-P

(A–C) Conformational landscape explored by MD simulations with EF-P (A), without EF-P (B), or with unmodified EF-P (C). The logarithm of the probability density ρ is shown along the two most dominant conformational modes of the CCA end and the C-terminal proline backbone atoms. Probability density maxima are indicated by crosses, green (simulations with EF-P, additionally marked with a square), red (without EF-P), and blue (unmodified EF-P). For comparison, plus signs (+) indicate the projections of our cryo-EM derived structure (black), the pre-attack state (Polikanov et al., 2014) (gray), and the uninduced and the induced states (Schmeing et al., 2005) (cyan and magenta, respectively).

(D–F) Conformations of P-site tRNA with peptide and EF-P corresponding to the density maxima obtained from MD simulations with EF-P (D; green), without EF-P (E; red) and with unmodified EF-P (F; blue). The cryo-EM structure with EF-P (black) and the pre-attack (Polikanov et al., 2014) (gray) conformation are shown for comparison. Distance between the ester carbonyl carbon of the peptidyl-tRNA and the α-amino group of the aa-tRNA is indicated in orange.

See also Figure S7.

By contrast, the overall position and interactions of the modified K34 residue of *E. coli* EF-P differs dramatically from that of the unmodified R32 residues of *T. thermophilus* EF-P (Blaha et al., 2009), which is significantly shorter and interacts only with the nucleobase of C75 of the P-site tRNA (Figure S3H).

The Conformation of the Nascent Chain in the Presence of EF-P

The presence of additional density for the nascent polypeptide chain attached to the P-site tRNA (Figures 5C and 5D) suggests that by stabilizing the P-site tRNA, EF-P also indirectly stabilizes the nascent chain. Nevertheless, local resolution calculations indicate that the nascent chain is still relatively flexible (Figure 5C), permitting only the four C-terminal residues to be

of A76 (Figure 5B). Furthermore, the hydroxyl group that is post-translationally added to K34 of EF-P by EpmC (Peil et al., 2012) comes within hydrogen binding distance of the 2′ OH of C74, but this interaction is unlikely to be critical since EF-P lacking the hydroxylation retains rescue activity (Doerfel et al., 2013; Ude et al., 2013; Peil et al., 2013). In addition, the EF-P modification can form hydrogen bonds with the conserved nucleotide A2439 of the 23S rRNA (Figure 5B), analogous to those formed between eIF5A and A2808 (Schmidt et al., 2016; Melnikov et al., 2016b), the equivalent residue in the yeast 28S rRNA (Figure S3I).

tentatively modeled into the density (Figure 5D). To compare the C-terminal Pro-Pro residues in our structure to other known conformations of Pro-Pro peptides, we initially aligned the X-ray structure of a short CCA-Pro-Pro tRNA mimic bound to the yeast 80S ribosome (Melnikov et al., 2016a) (Figure 5E). These two proline residues adopt an all-*trans* conformation, which is present in type II polyproline helices (Figure 5F) and also observed in other diprolyl-containing proteins, such as ribosomal proteins S11 and L11 (Fischer et al., 2015), and the ribosome-bound antimicrobial peptide Onc112 (Seefeldt et al., 2015; Roy et al., 2015)
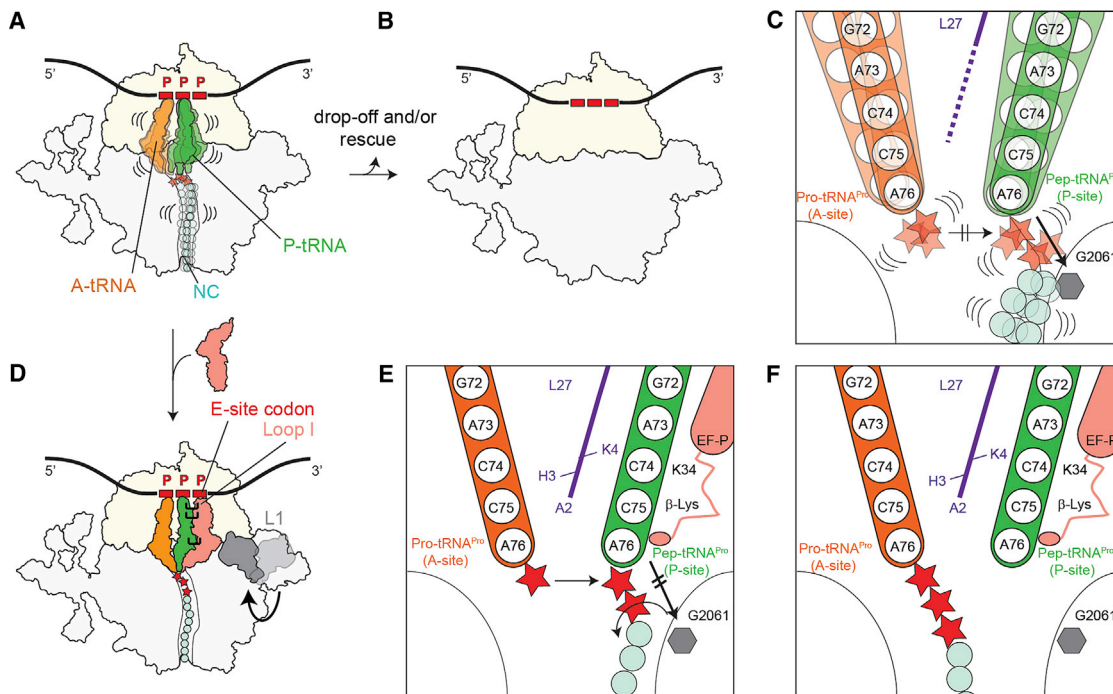
Figure 7. Mechanism of Action of EF-P on Polyproline-Stalled Ribosomes

(A and B) Ribosomes stall during translation of proteins containing three consecutive prolines (Doerfel et al., 2013; Ude et al., 2013) leading to destabilization of the peptidyl-tRNA in the P site (A), which leads to peptidyl-tRNA drop-off, particular with short peptidyl-tRNAs (Doerfel et al., 2013) (B).

(C) The all-*trans* or all-*cis* conformation of polyprolines (red stars) of the nascent chain is not possible because of a steric clash with G2061 (gray) within the tunnel wall, leading to peptidyl-tRNA destabilization and thus preventing accommodation of the A-site tRNA and peptide bond formation.

(D) Ribosomes stalled on polyproline stretches are recognized by EF-P, which binds within the E-site region and stabilizes the peptidyl-tRNA. EF-P binding is facilitated via contacts with the L1 stalk (Blaha et al., 2009) and the P-site tRNA (Katoh et al., 2016) as well as E-site codon.

(E) Interaction of the ε(R)-β-lysyl-hydroxylysine with the CCA end of P-site tRNA^Pro stabilizes the P-site tRNA, as well as the nascent chain, by forcing the prolines to adopt an alternative conformation that passes into the ribosomal exit tunnel.

(F) Thus, an optimal geometry between the nascent chain and the aminoacyl-tRNA in the A site is achieved and peptide bond formation can occur.

(Figures S6A–S6C). However, this conformation cannot occur on the ribosome because it would produce a steric clash between the −2 residue of the nascent chain and nucleotide G2061 of the 23S rRNA that comprises part of the ribosomal exit tunnel (Figure 5F; Figures S6A–S6C). Similarly, an all-*cis* conformation of the two prolyl residues is compatible neither with the density nor with translation, since it directs the nascent chain into the ribosomal A site (Figure 5G). Instead, the diprolyl moiety appears to adopt an alternative *trans*-conformation, allowing the −2 residue of the nascent chain to bypass G2061 and extend into the lumen of the ribosomal exit tunnel (Figure 5D). Although higher resolution will be required to accurately describe the *trans*-conformation in detail, our model suggests that the backbone Psi angle of ~120° is identical with the all-*trans* conformation, but the Phi angle of approximately −90° differs by ~30° from the all-*trans* Phi angle (−60°). Although the structure represents a "rescued state," the alternative conformation appears to be similar to that observed on a ribosome stalled by the diprolyl-containing, CMV-stalling peptidyl-tRNA (Matheisl et al., 2015) (Figure S6D), and the overall path of the nascent chain is similar to that observed for other stalling nascent polypeptide chains observed on the ribosome, such as TnaC (Bischoff et al., 2014), VemP (Su et al., 2017), MifM (Sohmen et al., 2015), and SecM (Zhang et al., 2015) (Figures S6E and S6F).

We note that when the rigid five-membered proline ring is replaced with a more flexible four-membered ring, such as in azetidine-2-carboxylic, ribosome stalling was reduced (Doerfel et al., 2015; Shin et al., 2017), possibly indicating that the additional freedom of the azetidine-2-carboxylic allows alternative conformations to be adopted more easily that do not sterically clash with G2061. In summary, we suggest that the incompatibility between the preferred diprolyl conformation of the nascent chain and the ribosome induces a strained conformation that can be relieved either by (1) destabilization of the P-site peptidyl-tRNA and therefore ribosomal stalling ensues or (2) binding of EF-P that stabilizes the P-site peptidyl-tRNA and forces the nascent chain to adopt an alternative conformation, with the outcome that peptide bond formation can occur.

EF-P Stabilizes the P-Site tRNA in a Pre-attack Conformation

To assess the dynamics of the region surrounding the PTC in the presence of modified EF-P or unmodified EF-P or the absence of EF-P, we carried out all-atom explicit-solvent molecular dynamics (MD) simulations. The first MD simulation was initiated using the model of the cryo-EM structure of the NlpD-PP-EF-P-ribosome, and two subsequent simulations were performed

where either the β-lysine part of modification on K34 or the entire EF-P protein were computationally removed. A total of 15 simulations, 2 μs each, accumulating to a total simulation run time of 30 μs were performed using a reduced system encompassing a 35 Å radius from the PTC. Principal-component analysis (PCA) (Amadei et al., 1993) was used to extract the two most dominant conformational modes of motion. As shown in Figure 6A, in the presence of modified EF-P, the major conformations are stable and remain close to the cryo-EM structure, which is similar to that observed in the X-ray structures of the *T. thermophilus* pre-attack conformation (Polikanov et al., 2014) as well as uninduced and induced conformations from *H. marismortui* (Schmeing et al., 2005). By contrast, after the β-lysine modification of EF-P or the complete EF-P protein was removed from the simulation, the system explored new conformations, moving away from the conformations observed in presence of EF-P, particularly with respect to conformational mode 2 (Figure 6C). Since conformational mode 2 reflects the relative distance between the α-amino group of an aminoacyl-tRNA in the A site and the carbonyl-carbon of the aminoacyl ester linkage in the peptidyl-Pro-Pro-tRNA (Figure S7), the MD simulations suggest that when the EF-P modification or the entire EF-P protein was absent, the peptidyl-tRNA moved away from the A-site tRNA, generating a geometry that is incompatible with peptide bond formation (Figures 6E and 6F). By contrast, the presence of the EF-P modification stabilized the pre-attack conformation of the P-site tRNA, thus promoting peptide bond formation (Figure 6D).

DISCUSSION

Collectively, our biochemical and structural findings, together with the available literature, lead us to propose a model for polyproline-mediated translational stalling and rescue by EF-P (Figure 7). Ribosomes translating proteins containing polyproline-stretches become stalled because of slow peptide bond formation between the peptidyl-Pro-Pro-tRNA in the P site and the incoming Pro-tRNA in the A site (Doerfel et al., 2013) (Figure 7A). The favorable all-*trans* conformation of the Pro-Pro peptide is not possible within the context of the ribosomal tunnel, which leads to destabilization of the P-site tRNA and nascent chain (Figure 7B). For short oligo-peptidyl-tRNAs, this results in high levels of peptidyl-tRNA drop-off (Doerfel et al., 2013, 2015). For longer peptidyl-tRNAs that are more refractory to drop-off, the destabilized peptidyl-tRNA results in suboptimal positioning for peptide bond formation and may also disfavor accommodation of the aminoacyl-tRNA at the A site (Figure 7B). Additionally, the destabilized peptidyl-tRNAs may be more susceptible to peptide release and/or ribosome rescue systems (Figures 7A and 7B), which may explain the unusually high proportion (30%) of vacant 70S ribosomes that were present in the PPP-stalled ribosome sample following purification (Figure S1A). Polyproline-stalled ribosomes are recognized by EF-P, which utilizes features of the E site codon of the mRNA, as well as specific interactions with D-loop of the P-site Pro-tRNA (Katoh et al., 2016), the L1 stalk, and the 30S subunit to promote binding (Blaha et al., 2009) (Figure 7C). While the presence of EF-P generally stabilizes the binding of the P-site tRNA, the ε(R)-β-lysylhydroxylysine is necessary to specifically interact and stabilize the CCA end at

the PTC (Figure 7D). Stabilization of the CCA end by the ε(R)-β-lysylhydroxylysine modification of EF-P also positions the nascent polypeptide chain such that it extends into the lumen of the tunnel (Figure 7E), thus allowing the CCA ends of the tRNAs to adopt the conformation that favors peptide bond formation (Figure 7F). These findings provide a structural rationale for the entropic steering effect of EF-P on peptide bond formation (Doerfel et al., 2015). It will be interesting to see how the distinct modifications found on EF-P in other bacteria, such as the rhamnosylation found in *P. aeurignosa* EF-P (Lassak et al., 2015; Rajkovic et al., 2015) or the 5-aminopentanol moiety of *B. subtilis* EF-P (Rajkovic et al., 2016), stabilize the CCA end of the P-site tRNA to promote an optimal geometry for peptide bond formation. Moreover, although it remains to be determined as to what promotes EF-P dissociation from the ribosome following peptide bond formation, our structure suggests that subunit rotation and opening of the L1 stalk are good candidates for destabilization of EF-P binding.

STAR★METHODS

Detailed methods are provided in the online version of this paper and include the following:

- KEY RESOURCES TABLE
- CONTACT FOR REAGENT AND RESOURCE SHARING
- EXPERIMENTAL MODEL AND SUBJECT DETAILS
  - ○ *E. coli* Strain and Growth Conditions
- METHODS DETAILS
  - ○ Preparation of the *E. coli Δefp* S12 Translation Extract
  - ○ PCR and *In Vitro* Transcription
  - ○ Preparation of Full-Length NlpD-PPP-SRC and Truncated NlpD-PP-SRC
  - ○ Purification of the NlpD-PPP-SRC and Truncated NlpD-PP-SRC
  - ○ Cryogrid Preparation for the NlpD-PPP-SRC and NlpD-PP-SRC
  - ○ Generation and Purification of Modified EF-P and Mutants
  - ○ Luminescence Determination of Firefly Luciferase
  - ○ Ribosome Complexes for Kinetic Experiments
  - ○ *In Vitro* Translation of fMPPPF Model Peptide
  - ○ Molecular Dynamics Simulations
  - ○ Conformational Landscape of CCA End and C-Terminal Proline
  - ○ Cryo-electron Microscopy and Single Particle Reconstruction
  - ○ Molecular Modeling and Map-Docking Procedures
  - ○ Figure Preparation
- QUANTIFICATION AND STATISTICAL ANALYSIS
  - ○ Cryo-EM Data Analysis
- DATA AND SOFTWARE AVAILABILITY
  - ○ Accession Numbers

SUPPLEMENTAL INFORMATION

Supplemental Information includes seven figures and can be found with this article online at https://doi.org/10.1016/j.molcel.2017.10.014.

REFERENCES

Adams, P.D., Afonine, P.V., Bunkóczi, G., Chen, V.B., Davis, I.W., Echols, N., Headd, J.J., Hung, L.W., Kapral, G.J., Grosse-Kunstleve, R.W., et al. (2010). PHENIX: a comprehensive Python-based system for macromolecular structure solution. Acta Crystallogr. D Biol. Crystallogr. *66*, 213–221.

Aduri, R., Psciuk, B.T., Saro, P., Taniga, H., Schlegel, H.B., and SantaLucia, J. (2007). AMBER force field parameters for the naturally occurring modified nucleosides in RNA. J. Chem. Theory Comput. *3*, 1464–1475.

Amadei, A., Linssen, A.B., and Berendsen, H.J. (1993). Essential dynamics of proteins. Proteins *17*, 412–425.

Arenz, S., Meydan, S., Starosta, A.L., Berninghausen, O., Beckmann, R., Vázquez-Laslop, N., and Wilson, D.N. (2014a). Drug sensing by the ribosome induces translational arrest via active site perturbation. Mol. Cell *56*, 446–452.

Arenz, S., Ramu, H., Gupta, P., Berninghausen, O., Beckmann, R., Vázquez-Laslop, N., Mankin, A.S., and Wilson, D.N. (2014b). Molecular basis for erythromycin-dependent ribosome stalling during translation of the ErmBL leader peptide. Nat. Commun. *5*, 3501.

Arenz, S., Bock, L.V., Graf, M., Innis, C.A., Beckmann, R., Grubmüller, H., Vaiana, A.C., and Wilson, D.N. (2016a). A combined cryo-EM and molecular dynamics approach reveals the mechanism of ErmBL-mediated translation arrest. Nat. Commun. *7*, 12026.

Arenz, S., Juette, M.F., Graf, M., Nguyen, F., Huter, P., Polikanov, Y.S., Blanchard, S.C., and Wilson, D.N. (2016b). Structures of the orthosomycin antibiotics avilamycin and evernimicin in complex with the bacterial 70S ribosome. Proc. Natl. Acad. Sci. USA *113*, 7527–7532.

Bailly, M., and de Crécy-Lagard, V. (2010). Predicting the pathway involved in post-translational modification of elongation factor P in a subset of bacterial species. Biol. Direct *5*, 3.

Behshad, E., Ruzicka, F.J., Mansoorabadi, S.O., Chen, D., Reed, G.H., and Frey, P.A. (2006). Enantiomeric free radicals and enzymatic control of stereo-

chemistry in a radical mechanism: the case of lysine 2,3-aminomutases. Biochemistry *45*, 12639–12646.

Berendsen, H.J.C., Postma, J.P.M., Van Gunsteren, W.F., Dinola, A., and Haak, J.R. (1984). Molecular dynamics with coupling to an external bath. J. Chem. Phys. *81*, 3684.

Berendsen, H.J.C., Grigera, J.R., and Straatsma, T.P. (1987). The missing term in effective pair potentials. J. Phys. Chem. *91*, 6269–6271.

Bischoff, L., Berninghausen, O., and Beckmann, R. (2014). Molecular basis for the ribosome functioning as an L-tryptophan sensor. Cell Rep. *9*, 469–475.

Blaha, G., Stanley, R.E., and Steitz, T.A. (2009). Formation of the first peptide bond: the structure of EF-P bound to the 70S ribosome. Science *325*, 966–970.

Bock, L.V., Blau, C., Schröder, G.F., Davydov, I.I., Fischer, N., Stark, H., Rodnina, M.V., Vaiana, A.C., and Grubmüller, H. (2013). Energy barriers and driving forces in tRNA translocation through the ribosome. Nat. Struct. Mol. Biol. *20*, 1390–1396.

Brown, A., Long, F., Nicholls, R.A., Toots, J., Emsley, P., and Murshudov, G. (2015). Tools for macromolecular model building and refinement into electron cryo-microscopy reconstructions. Acta Crystallogr. D Biol. Crystallogr. *71*, 136–153.

Bussi, G., Donadio, D., and Parrinello, M. (2007). Canonical sampling through velocity rescaling. J. Chem. Phys. *126*, 014101.

Chen, J.Z., and Grigorieff, N. (2007). SIGNATURE: a single-particle selection system for molecular electron microscopy. J. Struct. Biol. *157*, 168–173.

Chen, V.B., Arendall, W.B., 3rd, Headd, J.J., Keedy, D.A., Immormino, R.M., Kapral, G.J., Murray, L.W., Richardson, J.S., and Richardson, D.C. (2010). MolProbity: all-atom structure validation for macromolecular crystallography. Acta Crystallogr. D Biol. Crystallogr. *66*, 12–21.

Dever, T.E., Gutierrez, E., and Shin, B.S. (2014). The hypusine-containing translation factor eIF5A. Crit. Rev. Biochem. Mol. Biol. *49*, 413–425.

Doerfel, L.K., Wohlgemuth, I., Kothe, C., Peske, F., Urlaub, H., and Rodnina, M.V. (2013). EF-P is essential for rapid synthesis of proteins containing consecutive proline residues. Science *339*, 85–88.

Doerfel, L.K., Wohlgemuth, I., Kubyshkin, V., Starosta, A.L., Wilson, D.N., Budisa, N., and Rodnina, M.V. (2015). Entropic contribution of elongation factor P to proline positioning at the catalytic center of the ribosome. J. Am. Chem. Soc. *137*, 12997–13006.

Emsley, P., and Cowtan, K. (2004). Coot: model-building tools for molecular graphics. Acta Crystallogr. D Biol. Crystallogr. *60*, 2126–2132.

Essmann, U., Perera, L., Berkowitz, M.L., Darden, T., Lee, H., and Pedersen, L.G. (1995). A smooth particle mesh ewald method. J. Chem. Phys. *103*, 8577–8593.

Feenstra, K.A., Hess, B., and Berendsen, H.J.C. (1999). Improving efficiency of large time-scale molecular dynamics simulations of hydrogen-rich systems. J. Comput. Chem. *20*, 786–798.

Fischer, N., Neumann, P., Konevega, A.L., Bock, L.V., Ficner, R., Rodnina, M.V., and Stark, H. (2015). Structure of the E. coli ribosome-EF-Tu complex at <3 Å resolution by Cs-corrected cryo-EM. Nature *520*, 567–570.

Gutierrez, E., Shin, B.S., Woolstenhulme, C.J., Kim, J.R., Saini, P., Buskirk, A.R., and Dever, T.E. (2013). eIF5A promotes translation of polyproline motifs. Mol. Cell *51*, 35–45.

Hanawa-Suetsugu, K., Sekine, S., Sakai, H., Hori-Takemoto, C., Terada, T., Unzai, S., Tame, J.R., Kuramitsu, S., Shirouzu, M., and Yokoyama, S. (2004). Crystal structure of elongation factor P from *Thermus thermophilus* HB8. Proc. Natl. Acad. Sci. USA *101*, 9595–9600.

Hess, B. (2008). P-LINCS:cA parallel linear constraint solver for molecular simulation. J. Chem. Theory Comput. *4*, 116–122.

Hildebrand, A., Remmert, M., Biegert, A., and Söding, J. (2009). Fast and accurate automatic structure prediction with HHpred. Proteins *77* (*Suppl 9*), 128–132.

Johansson, M., Ieong, K.W., Trobro, S., Strazewski, P., Åqvist, J., Pavlov, M.Y., and Ehrenberg, M. (2011). pH-sensitivity of the ribosomal peptidyl

transfer reaction dependent on the identity of the A-site aminoacyl-tRNA. Proc. Natl. Acad. Sci. USA *108*, 79–84.

Joung, I.S., and Cheatham, T.E., 3rd (2008). Determination of alkali and halide monovalent ion parameters for use in explicitly solvated biomolecular simulations. J. Phys. Chem. B *112*, 9020–9041.

Katoh, T., Wohlgemuth, I., Nagano, M., Rodnina, M.V., and Suga, H. (2016). Essential structural elements in tRNA(Pro) for EF-P-mediated alleviation of translation stalling. Nat. Commun. *7*, 11657.

Lassak, J., Keilhauer, E.C., Fürst, M., Wuichet, K., Gödeke, J., Starosta, A.L., Chen, J.M., Søgaard-Andersen, L., Rohr, J., Wilson, D.N., et al. (2015). Arginine-rhamnosylation as new strategy to activate translation elongation factor P. Nat. Chem. Biol. *11*, 266–270.

Lassak, J., Wilson, D.N., and Jung, K. (2016). Stall no more at polyproline stretches with the translation elongation factors EF-P and IF-5A. Mol. Microbiol. *99*, 219–235.

Lindorff-Larsen, K., Piana, S., Palmo, K., Maragakis, P., Klepeis, J.L., Dror, R.O., and Shaw, D.E. (2010). Improved side-chain torsion potentials for the Amber ff99SB protein force field. Proteins *78*, 1950–1958.

Matheisl, S., Berninghausen, O., Becker, T., and Beckmann, R. (2015). Structure of a human translation termination complex. Nucleic Acids Res. *43*, 8615–8626.

Melnikov, S., Mailliot, J., Rigger, L., Neuner, S., Shin, B.S., Yusupova, G., Dever, T.E., Micura, R., and Yusupov, M. (2016a). Molecular insights into protein synthesis with proline residues. EMBO Rep. *17*, 1776–1784.

Melnikov, S., Mailliot, J., Shin, B.S., Rigger, L., Yusupova, G., Micura, R., Dever, T.E., and Yusupov, M. (2016b). Crystal structure of hypusine-containing translation factor eIF5A bound to a rotated eukaryotic ribosome. J. Mol. Biol. *428*, 3570–3576.

Muto, H., and Ito, K. (2008). Peptidyl-prolyl-tRNA at the ribosomal P-site reacts poorly with puromycin. Biochem. Biophys. Res. Commun. *366*, 1043–1047.

Navarre, W.W., Zou, S.B., Roy, H., Xie, J.L., Savchenko, A., Singer, A., Edvokimova, E., Prost, L.R., Kumar, R., Ibba, M., and Fang, F.C. (2010). PoxA, yjeK, and elongation factor P coordinately modulate virulence and drug resistance in *Salmonella enterica*. Mol. Cell *39*, 209–221.

Parrinello, M., and Rahman, A. (1981). Polymorphic transitions in single crystals: a new molecular dynamics method. J. Appl. Phys. *52*, 7182.

Pavlov, M.Y., Watts, R.E., Tan, Z., Cornish, V.W., Ehrenberg, M., and Forster, A.C. (2009). Slow peptide bond formation by proline and other N-alkylamino acids in translation. Proc. Natl. Acad. Sci. USA *106*, 50–54.

Peil, L., Starosta, A.L., Virumäe, K., Atkinson, G.C., Tenson, T., Remme, J., and Wilson, D.N. (2012). Lys34 of translation elongation factor EF-P is hydroxylated by YfcM. Nat. Chem. Biol. *8*, 695–697.

Peil, L., Starosta, A.L., Lassak, J., Atkinson, G.C., Virumäe, K., Spitzer, M., Tenson, T., Jung, K., Remme, J., and Wilson, D.N. (2013). Distinct XPPX sequence motifs induce ribosome stalling, which is rescued by the translation elongation factor EF-P. Proc. Natl. Acad. Sci. USA *110*, 15265–15270.

Pelechano, V., and Alepuz, P. (2017). eIF5A facilitates translation termination globally and promotes the elongation of many non polyproline-specific tripeptide sequences. Nucleic Acids Res. *45*, 7326–7338.

Pettersen, E.F., Goddard, T.D., Huang, C.C., Couch, G.S., Greenblatt, D.M., Meng, E.C., and Ferrin, T.E. (2004). UCSF Chimera–a visualization system for exploratory research and analysis. J. Comput. Chem. *25*, 1605–1612.

Polikanov, Y.S., Steitz, T.A., and Innis, C.A. (2014). A proton wire to couple aminoacyl-tRNA accommodation and peptide-bond formation on the ribosome. Nat. Struct. Mol. Biol. *21*, 787–793.

Pronk, S., Páll, S., Schulz, R., Larsson, P., Bjelkmar, P., Apostolov, R., Shirts, M.R., Smith, J.C., Kasson, P.M., van der Spoel, D., et al. (2013). GROMACS 4.5: a high-throughput and highly parallel open source molecular simulation toolkit. Bioinformatics *29*, 845–854.

Rajkovic, A., Erickson, S., Witzky, A., Branson, O.E., Seo, J., Gafken, P.R., Frietas, M.A., Whitelegge, J.P., Faull, K.F., Navarre, W., et al. (2015). Cyclic

rhamnosylated elongation factor P establishes antibiotic resistance in Pseudomonas aeruginosa. MBio *6*, e00823.

Rajkovic, A., Hummels, K.R., Witzky, A., Erickson, S., Gafken, P.R., Whitelegge, J.P., Faull, K.F., Kearns, D.B., and Ibba, M. (2016). Translation control of swarming proficiency in Bacillus subtilis by 5-amino-pentanolylated elongation factor P. J. Biol. Chem. *291*, 10976–10985.

Rohou, A., and Grigorieff, N. (2015). CTFFIND4: fast and accurate defocus estimation from electron micrographs. J. Struct. Biol. *192*, 216–221.

Roy, R.N., Lomakin, I.B., Gagnon, M.G., and Steitz, T.A. (2015). The mechanism of inhibition of protein synthesis by the proline-rich peptide oncocin. Nat. Struct. Mol. Biol. *22*, 466–469.

Scheres, S.H. (2012). RELION: implementation of a Bayesian approach to cryo-EM structure determination. J. Struct. Biol. *180*, 519–530.

Schmeing, T.M., Huang, K.S., Strobel, S.A., and Steitz, T.A. (2005). An induced-fit mechanism to promote peptide bond formation and exclude hydrolysis of peptidyl-tRNA. Nature *438*, 520–524.

Schmidt, C., Becker, T., Heuer, A., Braunger, K., Shanmuganathan, V., Pech, M., Berninghausen, O., Wilson, D.N., and Beckmann, R. (2016). Structure of the hypusinylated eukaryotic translation factor eIF-5A bound to the ribosome. Nucleic Acids Res. *44*, 1944–1951.

Schuller, A.P., Wu, C.C., Dever, T.E., Buskirk, A.R., and Green, R. (2017). eIF5A functions globally in translation elongation and termination. Mol. Cell *66*, 194–205.e5.

Seefeldt, A.C., Nguyen, F., Antunes, S., Pérébaskine, N., Graf, M., Arenz, S., Inampudi, K.K., Douat, C., Guichard, G., Wilson, D.N., and Innis, C.A. (2015). The proline-rich antimicrobial peptide Onc112 inhibits translation by blocking and destabilizing the initiation complex. Nat. Struct. Mol. Biol. *22*, 470–475.

Shin, B.S., Katoh, T., Gutierrez, E., Kim, J.R., Suga, H., and Dever, T.E. (2017). Amino acid substrates impose polyamine, eIF5A, or hypusine requirement for peptide synthesis. Nucleic Acids Res. *45*, 8392–8402.

Sohmen, D., Chiba, S., Shimokawa-Chiba, N., Innis, C.A., Berninghausen, O., Beckmann, R., Ito, K., and Wilson, D.N. (2015). Structure of the Bacillus subtilis 70S ribosome reveals the basis for species-specific stalling. Nat. Commun. *6*, 6941.

Starosta, A.L., Lassak, J., Peil, L., Atkinson, G.C., Virumäe, K., Tenson, T., Remme, J., Jung, K., and Wilson, D.N. (2014). Translational stalling at polyproline stretches is modulated by the sequence context upstream of the stall site. Nucleic Acids Res. *42*, 10711–10719.

Su, T., Cheng, J., Sohmen, D., Hedman, R., Berninghausen, O., von Heijne, G., Wilson, D.N., and Beckmann, R. (2017). The force-sensing peptide VemP employs extreme compaction and secondary structure formation to induce ribosomal stalling. eLife *6*, 6.

Ude, S., Lassak, J., Starosta, A.L., Kraxenberger, T., Wilson, D.N., and Jung, K. (2013). Translation elongation factor EF-P alleviates ribosome stalling at polyproline stretches. Science *339*, 82–85.

Voorhees, R.M., Weixlbaumer, A., Loakes, D., Kelley, A.C., and Ramakrishnan, V. (2009). Insights into substrate stabilization from snapshots of the peptidyl transferase center of the intact 70S ribosome. Nat. Struct. Mol. Biol. *16*, 528–533.

Vriend, G. (1990). WHAT IF: a molecular modeling and drug design program. J. Mol. Graph. *8*, 52–56, 29.

Wang, J., Wang, W., Kollman, P.A., and Case, D.A. (2006). Automatic atom type and bond type perception in molecular mechanical calculations. J. Mol. Graph. Model. *25*, 247–260.

Wohlgemuth, I., Brenner, S., Beringer, M., and Rodnina, M.V. (2008). Modulation of the rate of peptidyl transfer on the ribosome by the nature of substrates. J. Biol. Chem. *283*, 32229–32235.

Woolstenhulme, C.J., Parajuli, S., Healey, D.W., Valverde, D.P., Petersen, E.N., Starosta, A.L., Guydosh, N.R., Johnson, W.E., Wilson, D.N., and Buskirk, A.R. (2013). Nascent peptides that block protein synthesis in bacteria. Proc. Natl. Acad. Sci. USA *110*, E878–E887.

Yanagisawa, T., Sumida, T., Ishii, R., Takemoto, C., and Yokoyama, S. (2010). A paralog of lysyl-tRNA synthetase aminoacylates a conserved lysine residue in translation elongation factor P. Nat. Struct. Mol. Biol. *17*, 1136–1143.

Zhang, J., Pan, X., Yan, K., Sun, S., Gao, N., and Sui, S.-F. (2015). Mechanisms of ribosome stalling by SecM at multiple elongation steps. eLife *4*, 4.

Zheng, S.Q., Palovcak, E., Armache, J.P., Verba, K.A., Cheng, Y., and Agard, D.A. (2017). MotionCor2: anisotropic correction of beam-induced motion for improved cryo-electron microscopy. Nat. Methods *14*, 331–332.

Zhou, J., Korostelev, A., Lancaster, L., and Noller, H.F. (2012). Crystal structures of 70S ribosomes bound to release factors RF1, RF2 and RF3. Curr. Opin. Struct. Biol. *22*, 733–742.

STAR★METHODS

KEY RESOURCES TABLE

REAGENT or RESOURCE	SOURCE	IDENTIFIER
Bacterial and Virus Strains		
E. coli BL21(DE3)pLysS	Merck	69450
E. coli Δ*efp*	KEIO Collection	BW25113
Biological Samples		
tRNA from E.coli MRE600	Roche	10109550001
Chemicals, Peptides, and Recombinant Proteins		
Ampicillin	Sigma	A9518
Complete, EDTA-free	Roche	05056489001
Dpn 1	NEB	R0176S
GTP	Sigma	G8877
Isopropyl-β-D-1-thiogalactopyranoside	Roth	2316
Kanamycin	Sigma	60615
KOD Xtreme Hot Start Polymerase	Merck	71975
LiCl precipitation solution	Thermo Fisher Scientific	AM9480
n-Dodecyl b-D-maltoside (DDM)	Sigma	D4641
PEG-8000	Sigma	1546605
Phosphoenol pyruvate	Sigma	10108294001
Pyruvate kinase (PK)	Sigma	10109045001
Rnasin	Promega	N2511
rNTPs	Sigma	27-2025-01
Triton X-100	Sigma	T8787
Critical Commercial Assays		
Luciferase Assay System	Promega	E1500
PURExpress *In Vitro* Protein Synthesis Kit	New England Biolabs	E6800
Talon Purification kit	Clontech	635501
Deposited Data		
Dataset 1: Cryo-EM map of PPP stalled 70S with P-site tRNA	This paper	EMDB: 3900
Dataset 1: Cryo-EM map of PPP-stalled 70S with A+P-site tRNA	This paper	EMDB: 3901
Dataset 2: Cryo-EM map of EF-P/PPP-stalled 70S with P-site tRNA (no EF-P bound) and associated structural model	This paper	EMDB: 3898; PDB: 6ENF
Dataset 2: Cryo-EM map of EF-P/PPP-stalled 70S with A+P-site tRNA and EF-P and associated structural model	This paper	EMDB: 3899; PDB: 6ENJ
Dataset 3: Cryo-EM map of EF-P/PP stalled 70S with P-site tRNA and EF-P and associated structural model	This paper	EMDB: 3903; PDB: 6ENU
Dataset 3: Cryo-EM map of EF-P/PP stalled 70S with P+E-site tRNA (no EF-P bound)	This paper	EMDB: 3902
Oligonucleotides		
EF-P-R186A_FOR: 5′-GGTGAATACGTCTCTGCGGTGAAGTAATGGATC-3′	Eurofins Genomics	N/A
EF-P-R186A_REV: 5′-GATCCATTACTTCACCGCAGAGACGTATTCACC-3′	Eurofins Genomics	N/A
EF-P-Y183A_FOR: 5′-CCCGCTCTGGTGAAGCGGTCTCTCGCGTGAAG-3′	Eurofins Genomics	N/A
EF-P-Y183A_REV: 5′-CTTCACGCGAGAGACCGCTTCACCAGAGCGGG-3′	Eurofins Genomics	N/A
EF-P-loopID1_FOR: 5′-CTGAAAGGTGATACCGCAACTGGCGGCAAACCGGC-3′	Eurofins Genomics	N/A
EF-P-loopID1_REV: 5′-GCCGGTTTGCCGCCAGTTGCGGTATCACCTTTCAG-3′	Eurofins Genomics	N/A
EF-P-loopID2_FOR: 5′-GGCCTGAAAGGTGATACCACTGGCGGCAAACCGGC-3′	Eurofins Genomics	N/A
EF-P-loopID2_REV: 5′-GCCGGTTTGCCGCCAGTGGTATCACCTTTCAGGCC-3′	Eurofins Genomics	N/A

(Continued on next page)

REAGENT or RESOURCE	SOURCE	IDENTIFIER
EF-P-loopID3_FOR: 5′-CCGGGCCTGAAAGGTGATGGCGGCAAACCGGCTACC-3′	Eurofins Genomics	N/A
EF-P-loopID3_REV: 5′-GGTAGCCGGTTTGCCGCCATCACCTTTCAGGCCCGG-3′	Eurofins Genomics	N/A
EF-P-144AAA146_FOR: 5′-GATCCGGGCCTGAAAGCGGCGGCGGCAGGTACTG GCGGC-3′	Eurofins Genomics	N/A
EF-P-144AAA146_REV: 5′-GCCGCCAGTACCTGCCGCCGCCGCTTTCAGGC CCGGATC-3′	Eurofins Genomics	N/A
EF-P-K34A_FOR: 5′-CGTAAAACCGGGTGCGGGCCAGGCATTTG-3′	Eurofins Genomics	N/A
EF-P-K34A_REV: 5′-CAAATGCCTGGCCCGCACCCGGTTTTACG-3′	Eurofins Genomics	N/A
EF-P-DDomain3_FOR: 5′-GTTACTCCGCCGAACTAAGTTGAACTGGAAATC-3′	Eurofins Genomics	N/A
EF-P-DDomain3_REV: 5′-GATTTCCAGTTCAACTTAGTTCGGCGGAGTAAC-3′	Eurofins Genomics	N/A
Recombinant DNA		
Plasmid pET21b-R1NlpD	Starosta et al., 2014	N/A
pET46LIC_Ec_efp	Starosta et al., 2014	N/A
pRSFDuet_Ec_yjeK/Ec_yjeA	Starosta et al., 2014	N/A
Software and Algorithms		
WHATIF	Vriend, 1990	N/A
Gromacs 5, Solvate and GENION	Pronk et al., 2013	N/A
LINCS	Hess, 2008	N/A
SIGNATURE	Chen and Grigorieff, 2007	N/A
RELION-2	Scheres, 2012	N/A
CTFFIND4	Rohou and Grigorieff, 2015	N/A
MotionCor2	Zheng et al., 2017	N/A
Chimera	Pettersen et al., 2004	N/A
Coot	Emsley and Cowtan, 2004	N/A
Chem3Dpro	PerkinElmer	N/A
MolProbity	Chen et al., 2010	N/A
HHPred	Hildebrand et al., 2009	N/A
PyMol Molecular Graphic Systems Version 1.8	Schrödinger; https://pymol.org/2/	N/A
Other		
Protino Ni-NTA agarose beads	Macherey-Nagel	745400
Superdex HiLoad S75 16/600	GE Healthcare	28989333

CONTACT FOR REAGENT AND RESOURCE SHARING

Please direct any requests for further information or reagents to the Lead Contact, Daniel N. Wilson (daniel.wilson@chemie. uni-hamburg.de).

EXPERIMENTAL MODEL AND SUBJECT DETAILS

E. coli Strain and Growth Conditions
The *E. coli* Δ*efp* strain (Keio collection BW25113) was grown to OD_{600} = 5.8 in an 'INFORCE HT minifors' bench-top fermenter in 2xYPTG (16 g/l peptone, 10 g/l yeast extract, 5 g/l NaCl, 22 mM NaH_2PO_4, 40 mM Na_2HPO_4, 19.8 g/l glucose) at 37°C while maintaining pH 7.0 and oxygen level (60%).

METHODS DETAILS

Preparation of the *E. coli* Δ*efp* S12 Translation Extract
The *E. coli* Δ*efp* S12 translation extract was prepared as described for *B. subtilis* S12 translation extract (Sohmen et al., 2015) with some minor modifications. *E. coli* Δ*efp* cells (Keio collection BW25113) were grown to OD_{600} = 5.8 in an 'INFORCE HT minifors' bench-top fermenter in 2xYPTG (16 g/l peptone, 10 g/l yeast extract, 5 g/l NaCl, 22 mM NaH_2PO_4, 40 mM Na_2HPO_4, 19.8 g/l glucose) at 37°C while maintaining pH 7.0 and oxygen level (60%). Cells were collected at 5,000 x *g* at 4°C for 15 min. 22 g of cells were

resuspended in 14.6 mL of Buffer A (10 mM Tris-acetate, pH 8.2, 14 mM magnesium acetate, 60 mM potassium glutamate, 1 mM dithiothreitol and 6 mM 2-mercaptoethanol) and broken open in an 'microfluidics model 110I lab homogenizer', 3x at 15,000 psi. Subsequently, the lysate was cleared at 12,000 x g and incubated for 30 min at 37°C in a water bath. The cell extract was aliquoted, snap frozen and stored at −80°C.

PCR and *In Vitro* Transcription

Full-length *nlpD-PPP* construct with a N-terminal 6 x His- and HA-tag was amplified from pET-21b-$_{R1}$nlpD (Starosta et al., 2014) using T7 forward (5′-TAATACGACTCACTATAGGG-3′) and T7 terminator (5′GCTAGTTATTGCTCAGCGG-3′) primer. Truncated *nlpD-PP* construct was amplified from *nlpD-PPP* PCR product using T7 forward and revPP (5′-CGGCGGTCTAATCAACATAC-3′) primer. To avoid contamination with remaining full-length *nlpD-PPP* product, *nlpD-PP* was excised from the agarose gel and a second PCR was performed using the excised product as a template with T7 forward and revPP as primers. PCR products were purified and *in vitro* transcription reaction was performed using 2 μg of PCR product and 4μl of homemade T7 polymerase per 100 μl reaction volume (40 mM Tris pH 7.9, 25 mM Spermidine, 26 mM MgCl$_2$, 0,01% Triton X-100, 5mM DTT and 6.25 mM rNTPs (Sigma)) (Sohmen et al., 2015). The RNA was purified by LiCl/ethanol precipitation.

Preparation of Full-Length NlpD-PPP-SRC and Truncated NlpD-PP-SRC

Full-length NlpD-PPP-SRC was prepared using *E. coli* Δ*efp* S12 translation extract following the procedure described for the *B. subtilis* MifM-SRC (Sohmen et al., 2015). In summary the translation reaction contained 240 mM HEPES pH 8.2, 1.5 mM glucose, 2% PEG-8000, 2 mM DTT, 90 mM potassium glutamate, 80 mM ammonium acetate, 7.5 mM MgAc, 20 mM KH$_2$PO$_4$, 35 mM of each amino acid and 6.75 μl/25 μl of the S12 cell extract as well as 1.5 μl/25 μl reaction of *in vitro* transcribed mRNA. For the purifications of the SRCs the reaction was scaled up to 2500 μl. *In vitro* translation was carried out for 20 min. Translation reaction was stopped by adding ice cold Buffer B (50 mM HEPES pH 7.2 at 4°C, 250 mM KOAc, 10 mM MgOAc, 0,1% DDM, 1/1,000 complete protease inhibitor (Roche), 0.2 U/ml RNasin). For the truncated NlpD-PP-SRC, the *in vitro* reaction was carried out using PURExpress *In vitro* Protein Synthesis Kit (NEB). The translation reaction (750 μl in total) was prepared according to the protocol of the PURExpress *In vitro* Protein Synthesis Kit but was supplemented with 5 μM anti-ssrA oligo (5′TTAAGCTGCTAAAGCGTAGTTTTCG TCGTTTGCGACTA-3′). Translation was started by adding the truncated *nlpD-PP* PCR product and then the reaction was incubated at 37°C for 20 min with shaking at 1,000 rpm.

Purification of the NlpD-PPP-SRC and Truncated NlpD-PP-SRC

Translation reactions were loaded onto 500 mL sucrose cushion (750 mM sucrose) in Buffer B and pelleted at a speed of 45.000 rpm for 150 min in a TLA 120.2 rotor (Sohmen et al., 2015). The SRCs were resuspended in Buffer B and bound via its N-terminal 6x His-tag to a Talon metal affinity chromatography column (Clontech) which was pre-equilibrated with Buffer B containing 10 mg/ml bulk tRNA. The column was washed with Buffer C (same as Buffer B, but with 500 mM KOAc). The SRCs were eluted by using Buffer B supplemented with 150 mM Imidazole. The eluates were loaded onto 10%–40% sucrose gradients (in Buffer B) and centrifuged for 13h in a Beckman coulter SW40 swinging bucket rotor at 20.000 rpm. 70S peaks were collected, pelleted for 3h in a TLA 120.2 rotor (45.000 rpm) and pellets were resuspended in Buffer B. Purification of the SRCs were confirmed by SDS-Page and western blotting using an anti-HA-tag antibody.

Cryogrid Preparation for the NlpD-PPP-SRC and NlpD-PP-SRC

Dataset 1: For grid preparation 4.5 OD A$_{260}$/ml monosomes of the full-length NlpD-PPP-SRC were used. Dataset 2: For grid preparation 5.0 OD A$_{260}$/ml monosomes of the full length NlpD-PPP-SRC were used and a 3x excess of modified EF-P over 70S was added and incubated for 20 min at 37°C. Dataset 3 For grid preparation 4.5 OD A$_{260}$/ml monosomes of the truncated NlpD-PP SRC were used. A 5x excess of modified EF-P over 70S as well as 100 μM evernimicin (to ensure absence of A-site tRNA) (Arenz et al., 2016b) were added and incubated for 5 min at 37°C. All samples were applied to 2 nm precoated Quantifoil R3/3 holey carbon supported grids and vitrified using a Vitrobot Mark IV (FEI company).

Generation and Purification of Modified EF-P and Mutants

All EF-P variants were generated by site-directed mutagenesis PCR using the whole plasmid PCR method with pET46LIC_EC_efp as a template (primers and plasmids are listed in the Key Resources Table). For the PCR reaction the KOD Xtreme Hot Start Polymerase (Merck) was used with the following conditions: 94°C 2 min; 20x (98°C 10 s, 63°C 30 s, 68°C 2 min); 68°C 7 min. The product was digested with Dpn1 (NEB) for 1h at 37°C and purified using a PCR Purification Kit (Qiaqen). The EF-P variants were coexpressed together with EpmA and EpmB from pRSFDuet vector (to ensure modification of EF-P) in *E. coli* BL21 cells grown at 37°C from overnight culture in lysogeny broth (LB) medium and in the presence of 100 μg/mL ampicillin and 50 μg/ml kanamycin. Protein expression was induced at an OD$_{600}$ of 0.4 with a final concentration of 1 mM isopropyl-β-D-1-thiogalactopyranoside (IPTG) (Roth). After 1 hour of expression cells were lysed using a microfluidizer. The cell lysate was cleared using a SS34 rotor at 4°C and 44,100 x g for 30 minutes. Purification of His-tagged proteins was done with Protino Ni-NTA agarose beads (Macherey-Nagel). The final eluate was applied onto a Superdex HiLoad S75 16/600 column (GE Healthcare) to yield the final concentrated protein in gel filtration buffer

(50 mM HEPES pH 7.4, 50 mM KCl, 100 mM NaCl and 5 mM 2-mercaptoethanol). The post-translational modification of wild-type EF-P and EF-P variants was confirmed by mass spectrometry as performed previously for EF-P (Peil et al., 2012).

Luminescence Determination of Firefly Luciferase
In vitro translation of the firefly luciferase was performed using the PURExpress *in vitro* translation kit. For template generation Fluc3xPro was amplified via PCR using T7 forward and T7 reverse primer from plasmid pIVEX-Fluc3xPro (Ude et al., 2013). Samples have been incubated at 37°C for defined time periods. 1 µl of each reaction were added on to white 96-well chimney flat bottom microtiter plates. 40 µl of luminol substrate (Promega) was added, immediately before luminescence was detected using a Tecan Infinite M1000.

Ribosome Complexes for Kinetic Experiments
The mRNA (GGGCAAGGAGGUAAAUA<u>AUGCCGCCGCCGUUC</u>AUU) coding for fMPPPF was synthesized by IBA Lifescience. Initiation complexes were formed by incubating 70S ribosomes (1 µM) with IF 1, IF2, IF3 (1.5 µM each), f[^{3}H]Met-tRNA^{fMet} (3 µM) and GTP (1 mM) in buffer D (50 mM Tris-HCl, pH 7.5 at 37°C, 70 mM NH$_4$Cl, 30 mM KCl and 7 mM MgCl$_2$) for 30 min (Doerfel et al., 2013). Initiation complexes were purified by centrifugation through a 400 µl sucrose cushion (40% sucrose in buffer D) at 260,000 g for 2 h at 4°C. Pellets were dissolved in buffer D, flash frozen and stored at −80°C. [^{14}C]Phe-tRNA^{Phe} was prepared from total tRNA as described. tRNA^{Pro} *in-vitro* transcripts were prepared and aminoacylated as described (Doerfel et al., 2013). Ternary complexes EF-Tu–GTP–aminoacyl-tRNA were prepared by incubating aminoacyl-tRNA (Pro-tRNA^{Pro} and Phe-tRNA^{Phe}) with a 2.5-fold excess of EF-Tu, GTP (1 mM), pyruvate kinase (0.1 µg/µl) and phosphoenolpyruvate (3 mM) for 15 min at 37°C.

In Vitro Translation of fMPPPF Model Peptide
Initiation complexes (0.2 µM), ternary complexes Pro and Phe (each 2 µM), EF-G (1 µM) and EF-P (varying concentrations) were mixed in buffer E (50 mM Tris-HCl, pH 7.5 at 37°C, 70 mM NH$_4$Cl, 30 mM KCl, 3.5 mM MgCl$_2$, 0.5 mM spermidine, 8 mM putrescine and 2 mM DTT) at 37°C. The reaction was quenched after 20 s with KOH (0.5 M), hydrolyzed for 30 min at 37°C and neutralized with glacial acetic acid. Amino acids and peptides were separated by reversed-phase HPLC (Chromolith Performance RP8e 100-4.6 column, Merck) using a 0%–65% acetonitrile gradient in 0.1% TFA. Products and educts were quantified by double-label scintillation counting (Doerfel et al., 2013).

Molecular Dynamics Simulations
To obtain the dynamics of the region surrounding the PTC in presence of EF-P, unmodified EF-P or without EF-P, we carried out all-atom explicit-solvent molecular dynamics (MD) simulations. The simulations were started (i) from the cryo-EM structure, (ii) from the cryo-EM structure after removal of the β-lysine modification of Lys34 (EF-P), and (iii) after removal of EF-P. Since the structural differences between the cryo-EM structures with and without EF-P are only found in the vicinity of the PTC, we used a reduced simulation system that allowed us to increase the achievable simulation time. The simulation system (+EF-P) includes all residues of the cryo-EM structure located within 35 Å of any atom of the P-site tRNA CCA tail, of the attached peptide, or of the β-lysine modified Lys34 of EF-P. Nucleotides (amino acids) that are not within this radius, but whose 5′- and 3′- (n- and c-) neighbors are within the radius, are also included in the simulation system. Nucleotides whose 5′ (3′) bound nucleotide neighbor is not in the simulation system were treated as 5′ (3′) terminal nucleotides. Any amino acid i whose i−1 neighbor (i + 1 neighbor) is not in the simulation system was capped by an uncharged N-terminal acetyl (C-terminal amide). Positions of residues in a 25 Å radius were not restrained (inner layer), while heavy atom positions of the remaining residues (outer layer) were restrained by a harmonic potential. The harmonic force constant k of each restrained atom was chosen as k = 8RT π · rmsf^2 where rmsf is the root mean square fluctuation of the corresponding atom obtained from a 2 µs-simulations of the full ribosome in complex with A- and P-site tRNAs and the ErmBL peptide (Arenz et al., 2016a). For those heavy atoms without corresponding atoms in the full-ribosome simulations, the average of all other force constants was used. Two more simulation systems were used, one after removal of the modification of EF-P Lys34 (+EF-P (unmod)) and the other after removal of all EF-P atoms (–EF-P). To place initial Mg^{2+} ions, a cryo-EM structure of the ribosome (Fischer et al., 2015) was aligned to each simulation system. Then, Mg^{2+} ions resolved in the cryo-EM structure that are located within 5 Å of the atoms of the simulation system were extracted from the aligned structure and included in the simulations system. WHATIF (Vriend, 1990) was used to determine the protonation states of the histidines. Each simulation systems was then solvated in a dodecahedron box of water molecules with a minimum distance of 1.5 nm between the atoms of the simulation system and the box boundaries using the program solvate (Pronk et al., 2013). To neutralize the overall charge of each system, first the Coulomb potential at the positions of all water oxygen atoms was calculated based on the charges and positions of all other atoms. Iteratively, the water molecule with the lowest Coulomb potential was replaced by a K$^+$ ion and the Coulomb potential at all other water oxygens was updated until the overall charge was neutral. Using the program GENION (Pronk et al., 2013), subsequently 7 mM MgCl$_2$ and 150 mM KCl were added. All simulations were carried out with Gromacs 5 (Pronk et al., 2013) using the amberff12sb force field (Lindorff-Larsen et al., 2010) and the SPC/E water model (Berendsen et al., 1987). Force field parameters for modified nucleotides were taken from (Aduri et al., 2007). Potassium and chloride ion parameters were taken from (Joung and Cheatham, 2008). Atom types for β-lysine modified Lys were obtained with ANTECHAMBER (Wang et al., 2006) and partial charges were determined using DFT-B3LYP with a 6-31/G* basis set. The ester bond between the C-terminal proline and A76 of the P-site tRNA was treated as described earlier (Bock et al.,

2013). Lennard- Jones and short-range Coulomb interactions were calculated within a distance of 1 nm, while long-range Coulomb interactions were calculated using particle-mesh Ewald summation (Essmann et al., 1995). The LINCS algorithm was used to constrain bond lengths (Hess, 2008) and virtual site constraints (Feenstra et al., 1999) were used for hydrogens, allowing an integration time step of 4 fs. Solute and solvent temperatures were controlled independently at 300 K using velocity rescaling (Bussi et al., 2007) with a coupling time constant of 0.1 ps. For each of the three simulation systems, the system was equilibrated in four steps. First, the potential energy was minimized using steepest decent while restraining the positions of all solute heavy atoms (k = 1000 kJ mol^{-1} nm^{-2}). Second, for the first 50 ns, the pressure was coupled to a Berendsen barostat (1 ps coupling time) (Berendsen et al., 1984) and position restraints were applied. Third, during the next 20 ns, the position restraint force constant was linearly decreased to the values obtained from the full-ribosome simulations for the outer-layer atoms and to zero for the remaining atoms. Finally, for production runs starting at 70 ns, the Parrinello-Rahman barostat was used (Parrinello and Rahman, 1981). At simulation times 170, 270, 370, and 470 ns coordinates were extracted from the trajectory, new velocities were assigned according to a Boltzmann distribution, and subsequently new simulations were started, resulting in a total of 15 simulations, 2 μs each, accumulating to a total production run simulation time of 30 μs.

Conformational Landscape of CCA End and C-Terminal Proline

To investigate how either the removal of the modification of EF-P or the removal of EF-P entirely changes the conformation of the P-site CCA end and the C-terminal proline of the peptide, we carried out a Principal Component Analysis (PCA) (Amadei et al., 1993). A PCA is used to extract the dominant modes of motion, here the first two eigenvectors. To that aim, we first aligned all the trajectories using all 23S P atoms and, second, extracted backbone atoms of the CCA end (O3′, C3′, C4′, C5′, O5′, and P atoms) and of the peptide (N, CA, C, and O atoms). The extracted trajectories were then concatenated and the atomic displacement covariance matrix was calculated. The eigenvectors of this covariance matrix were sorted according to their eigenvalues. The eigenvectors corresponding to the largest eigenvalues represent the most dominant conformational modes. To describe the structural ensembles obtained from the three sets of simulations, first, the projection of all the frames onto the first two eigenvectors was calculated. For each set of simulations, the projections were then sorted into 2-dimensional bins and the logarithm of the probability $\rho = c_{i,j}/c_{total}$ of each bin i,j was calculated, where $c_{i,j}$ is the number of the projections in the bin, c_{total} is the total number of frames (Figures 6A–6C). For comparison, our cryo-EM structure with EF-P as well the X-ray structures of the pre-attack conformation (Polikanov et al., 2014) and the uninduced and induced conformations (Schmeing et al., 2005) were projected onto the two conformational modes (Figures 6A–6C). For each set of simulations, all the structures sorted into the bin marked with a cross in the conformational landscape (Figures 6A–6C) were extracted. For each set, from the extracted structures the one with the median peptide bond distance was chosen and is shown in (Figures 6D–6F).

Cryo-electron Microscopy and Single Particle Reconstruction

Data collections were performed on FEI Titan Krios transmission electron microscopes equipped with a Falcon II direct electron detector (FEI) at 300 kV at a pixel size of 1.064 Å (Dataset 1) or 1.084 Å (Dataset 2 and 3). Dataset 1: Defocus range was from −1.0 to −2.5 μm (underfocus) resulting in 1156 Micrographs after manual inspection and discarding micrographs with resolution worse than 4 Å. Each micrograph contained 16 frames (2.68 e$^-$/Å^2). Original image stacks were motion-corrected and dose weighted using MotionCor2 (Zheng et al., 2017). Dataset 2 and 3: Defocus range was from −0.8 to −2.5 μm (underfocus) resulting in 2109 micrographs for Dataset 2 and 1957 micrographs for Dataset 3 after manual inspection and discarding micrographs showing a resolution worse than 3.3 Å (Dataset 2) and 3.4 Å (Dataset 3), respectively. Each micrograph contained 17 frames in total (2.4 e$^-$/Å^2 + 4 e$^-$/Å^2 pre exposure) and frames 0-9 were used resulting in a total dose of 28 e$^-$/Å^2. Original image stacks were motion-corrected using MotionCor2 (Zheng et al., 2017). Power-spectra, defocus values, astigmatism and estimation of resolution were determined using CTFFIND4 software (Rohou and Grigorieff, 2015). After automated particle picking using SIGNATURE (Chen and Grigorieff, 2007) single particles were processed using RELION-2 (Scheres, 2012). All particles from the three datasets (Dataset 1: 121,704 particles, Dataset 2: 229,613 particles, Dataset 3: 229,458 particles) were first subjected to 3D refinement using an *E. coli* 70S ribosome as reference structure and subsequently a 3D classification was performed (Figure S1). Dataset 1 was classified into four classes and dataset 2 and 3 into eight classes. For dataset 3 classes 2 and 3 were joined and a second classification was performed with a mask focusing on EF-P. Final structures of all datasets were refined, corrected for the modulation transfer function of the Falcon 2 detector and sharpened by applying a negative B-factor automatically estimated by RELION-2 (Figure S1). Resolution was estimated using the "gold standard" criterion (FSC = 0.143).

Molecular Modeling and Map-Docking Procedures

The molecular model for the ribosomal proteins and rRNA of either the PPP or PP stalled complexes is based on the molecular model for the 70S subunit from the cryo-EM reconstruction of the *E. coli* 70S ribosome (PDB: 5AFI) (Fischer et al., 2015) and obtained by performing a rigid body fit into the cryo-EM density map of the corresponding stalled complex using UCSF Chimera (Pettersen et al., 2004) (fit in map function). For *E. coli* EF-P, a homology model was generated using HHPred (Hildebrand et al., 2009) based on a template from *T. thermophilus* (PDB: 3HUW) (Blaha et al., 2009). The model was fitted to the density using Chimera (Pettersen et al., 2004) and refined in Coot (Emsley and Cowtan, 2004). The post-translational modification of ε(R)−β−lysylhydroxylysine that is positioned at K34 of EF-P was designed using Chem3DPro (PerkinElmer), manually placed into the cryo-EM density map at

position 34 of EF-P and refined in Coot. P-site tRNA of the *E. coli* 70S ribosome (PDB: 5AFI) (Fischer et al., 2015) was manually mutated to tRNA[Pro(CCG)]. In the case of the truncated PP-SRC in the presence of EF-P, the L1 stalk and L1 protein were taken from the crystal structure of *T. thermophilus* (PDB: 3HUW), manually mutated and refined using Coot. Nucleotides of the PTC that differ from the cryo-EM *E. coli* 70S ribosome (PDB: 5AFI) (Fischer et al., 2015) were manually refined into density using Coot. Atomic coordinates were refined using *phenix.real_space_refine* (Adams et al., 2010), with restraints obtained by *phenix.secondary_structure_restraints* (Adams et al., 2010). Cross-validation against overfitting was performed as described elsewhere (Brown et al., 2015). Statistics of the refined models were obtained using MolProbity (Chen et al., 2010) and are presented in Table 1.

Figure Preparation

Figures showing electron densities and atomic models were generated using either UCSF Chimera (Pettersen et al., 2004) or PyMol Molecular Graphic Systems (Version 1.8 Schrödinger). Figure panels were assembled using Adobe Illustrator.

QUANTIFICATION AND STATISTICAL ANALYSIS

Cryo-EM Data Analysis

Bayesian selection using RELION software package was used to choose the cryo-EM data package (Scheres, 2012). Resolutions were calculated according to gold standard and the estimation of variation within each group of data was performed using Bayesian calculation within RELION (Scheres, 2012).

DATA AND SOFTWARE AVAILABILITY

Accession Numbers

The atomic coordinates and/or the associated maps have been deposited in the PDB and/or EMDB with the accession codes EMD: 3900 (Dataset 1, P-tRNA only), EMD: 3901 (Dataset 1, A+P-tRNA), EMD: 3898/PDB: 6ENF (Dataset 2, P-tRNA only), EMD: 3899/PDB: 6ENJ (Dataset 2, A+P-tRNA+EF-P), EMD: 3903/PDB: 6ENU (Dataset 3, P-tRNA+EF-P) and EMD: 3902 (Dataset 3, P+E-tRNA).